esa

DOCUMENT

document title/ titre du document

PROBA3

ENVIRONMENTAL SPECIFICATION

prepared by/*préparé par* J. Sørensen

reference/*réference* P3-EST-RS-6003
issue/*édition* 1
revision/*révision* 1
date of issue/*date d'édition* 26 September 2008
status/*état*
Document type/*type de document*
Distribution/*distribution*

European Space Agency
Agence spatiale européenne

ESTEC
European Space Research and Technology Centre - Keplerlaan 1 - 2201 AZ Noordwijk - The Netherlands
Tel. (31) 71 5656565 - Fax (31) 71 5656040 www.esa.int

APPROVAL

Title *Titre*	PROBA 3 Environmental Specification	issue 1 *issue*	revision 0 *revision*

author *auteur*	J. Sørensen	date *date*
approved by *approuvé par*	F. Burger	date *date*

CHANGE LOG

reason for change /*raison du changement*	issue/*issue*	revision/*revision*	date/*date*
Initial issue	1	0	17/6-08
Added data on plasma and update of solar proton model		1	26/9-08

CHANGE RECORD

Issue: 1 Revision: 0

reason for change/*raison du changement*	page(s)/*page(s)*	paragraph(s)/*paragraph(s)*
Added data on plasma Update of solar proton model Update of references	1-2, 4, 6, 8, 11-13, 19, 22-30, 37-39, 41-43, 45-49, 53, 60, 70	

TABLE OF CONTENTS

1 INTRODUCTION

The Space Environment can cause severe problems for any space system including Proba3. Proper assessment of the potential effects is an essential part of the engineering process leading to the construction of any element of the spacecraft. It is important that this is taken into account from the earliest phases of a project when consideration is given to mass budget, protection, component selection policy, etc. As the design of an element is developed, further engineering iteration is normally necessary with more detailed analysis.

This document is prepared for the development of the Proba3 spacecraft. It is intended to assist the developers of both the payload and the spacecraft carrier in assessing the effects of the space environment on their systems. The document is based on the ECSS-E-ST-10-04C Space Environment Standard, from which most of the background information has been taken (ECSS is a cooperative effort of the European Space Agency, National Space Agencies and European industry associations for the purpose of developing and maintaining common standards). The ECSS-E-ST-10-04C standard can also be accessed via the WWW site:

http://www.esa.int/TEC/Space_Environment/index.html.

The ECSS standard [1] shall apply to all space environments and effects analyses. This defines appropriate analysis methods and models, including the ones employed here.

1.1 The Mission

The baseline operational orbit is a highly elliptical low inclination orbit with altitudes ranging from about 800km to 71000km. Proba3 is thus continuously crossing the radiation belts giving rise to a far more severe environment than the previous Proba1 and Proba2 spacecraft, which were in a low earth orbit. The nominal mission duration is 2 years. The planned launch date is in 2012.

The baseline orbit parameters are listed in table 1.

Table 1: Baseline orbit

Parameter	Value
Semi-major axis [km]	42378.144
Eccentricity	0.830617
Inclination [deg]	17.8
R.A. of ascending node [deg]	68.0
Argument of perigee [deg]	180.0
Mission duration [years]	2

A direct injection into the operational orbit is assumed.

1.2 The Space Environment

The environments included are:

- Solar and Planetary Electromagnetic Radiation
- Plasmas
- Energetic Particle Radiation
- Particulates
- Contamination

Each is treated in a separate chapter, although synergies and cross-linking of models are specified. The natural environment is described together with the general models in use and principles for determining the local induced environment. Although, also important, the thermal environment is not treated in this document (except for the external heat sources). Many of the models mentioned are also installed in the Space Environment Information System (Spenvis), which can be accessed via the WWW site http://www.spenvis.oma.be/spenvis/.

Since the Proba3 orbit is well outside the atmosphere, the neutral atmosphere is not described in this document.

For many of the associated analyses it is necessary to take the geometry of the spacecraft into account, but such geometrical analyses are out of the scope of this document.

1.3 References

[1] ECSS-E-ST-10-04C, Space Engineering, Space Environment

2 SOLAR AND EARTH ELECTROMAGNETIC RADIATION ENVIRONMENT AND SOLAR/GEOMAGNETIC INDICES

2.1 Introduction

The Proba3 spacecraft will in its orbit receive electromagnetic radiation from three primary external sources. The largest source is the direct solar flux. The mean value of this solar flux at the mean Sun-Earth distance is called the 'solar constant'. It is not really a constant but varies by about 3.4 % during each year because of the slightly elliptical orbit of the Earth about the sun.

The fraction of incident sunlight that is reflected off a planet is termed albedo. For an orbiting spacecraft the albedo value depends mainly on the sunlit part of the Earth which it can see. Albedo radiation has approximately the same spectral distribution as the sun here albedo refers to the total solar spectrum albedo. Albedo is highly variable across the globe and depends on surface properties and cloud cover. It also depends on the solar zenith angle.

The third source is the Earth infrared radiation. The Earth-emitted thermal radiation has a spectrum of a black body with a characteristic average temperature of 288 K. The Earth infrared radiation also varies across the globe but less than the albedo. It also shows a diurnal variation which is small over the ocean but can amount to 20 % for desert areas.

Solar and geomagnetic activities are often described by indices. The UV radiation of the sun, which strongly effects the Earth atmosphere, cannot be directly measured from the ground. But it was found to be strongly correlated with e.g. the sunspot number and the cm wavelength sun radiation. The widely used 10.7 cm radio flux index ($F_{10.7}$) gives a good measure of the solar UV radiation output which is highly variable over a solar cycle.

Geomagnetic indices typically describe the variation of the geomagnetic field over a certain time period. They provide a measure of the disturbance of the magnetosphere which has direct consequences for the charged particle space environment.

Solar and geomagnetic indices are required as input for upper atmosphere and other models of the near Earth space environment. They are provided for short durations or as long time averages. Predictions for future index values are usually provided at different confidence levels and they are available for complete solar cycles.

The given data are mainly average values. For detailed thermal analyses or certain special applications more detailed treatment is required, which is outside the scope of this document.

2.2 Solar electromagnetic radiation

2.2.1 SOLAR CONSTANT

The solar constant is defined as the radiation that falls on a unit area of surface normal to the line from the Sun, per unit time, outside the atmosphere, at one astronomical unit (1 AU = average Earth-Sun distance).

The solar constant has an uncertainty of about ± 3 W/m^2. The following values for the electromagnetic radiation shall be used:

Solar constant at 1 AU:	1366 W/m^2
Maximum solar energy flux (winter solstice):	1413 W/m^2
Minimum solar energy flux (summer solstice):	1322 W/m^2
Solar radiation pressure (100 % reflecting plate):	9.02×10^{-6} N/m^2

2.2.2 SOLAR SPECTRUM

The solar spectrum shall be approximated by a black body curve with a characteristic temperature of 5762K (this is the temperature that at 1AU gives the value of the solar constant reported above). A space sink temperature of 3 K shall be assumed.

The UV portion (wavelength, λ,< 300 nm) of the electromagnetic spectrum is of particular importance in determining effects of solar radiation on the upper atmosphere and on material properties. The integrated irradiance of the near UV electromagnetic radiation flux (180 nm < λ < 400 nm) is approximately 118 W/m^2. The far UV portion (λ < 180 nm) contributes about 0.023 W/m^2.

Certain parts of the spectrum are much more variable, both, over the 27-day solar rotation period and over the 11-year solar cycle. This variation ranges from about 50 % for the near UV part to a factor 2 for the UV and far UV portions and can reach orders of magnitude for flare X-rays.

Average and worst case irradiance levels for the high-energy spectrum are summarized in Table 1. The average values were taken from [1].

Table 1: High-energy solar electromagnetic flux

Type	**Wavelength (nm)**	**Average Flux (W/m^2)**	**Worst-Case Flux (W/m^2)**
Near UV	180-400	118	177
UV	< 180	2.3×10^{-2}	4.6×10^{-2}
UV	100-150	7.5×10^{-3}	1.5×10^{-2}
EUV	10-100	2×10^{-3}	4×10^{-3}
X-Rays	1-10	5×10^{-5}	1×10^{-4}
Flare X-Rays	0.1-1	1×10^{-4}	1×10^{-3}

For design purposes the worst case values of Table 1 shall be used. The fluxes given for flare X-rays are peak values of large flares. For design, one such X-ray flare per week, lasting one hour, shall be assumed.

Figure 1 shows the solar irradiation spectrum at sea level and outside the Earth atmosphere. More details on the solar spectrum can be found in [2], [3] and [4].

2.3 Earth electromagnetic radiation

2.3.1 EARTH ALBEDO

Albedo is the fraction of sunlight which is reflected off a planet. The average albedo of the Earth is about 0.3. For short periods the albedo can vary considerably between about 0.05 and 0.6.

For albedo radiation the same spectral shape as for sunlight shall be assumed. The actual albedo spectrum can change, depending on properties of the surface and atmosphere. Ground vegetation and atmospheric water and dust can lead to absorption in certain wavelength bands and result in a highly variable albedo spectrum.

Albedo values are only applicable when a portion of the Earth that is seen by the Proba3 spacecraft is sunlit. Albedo values vary with solar zenith angle. The sunlit part of the Earth and the solar zenith angle shall be considered for albedo analyses. Additional information on the variability of the albedo is given in [3].

2.3.2 EARTH INFRARED

The Earth-emitted thermal radiation is also called Earth Infrared or Outgoing Long-wave Radiation. For the Earth Infrared radiation a black body spectrum with a characteristic temperature of 288 K shall be assumed. The average infrared radiation emitted by Earth is 230 W/m^2. On a

short time scale it can vary between 150 to 350 W/m^2. The diurnal variations can amount to about 20 percent over desert areas while it is small over oceans. Additional information on the variability of the Earth infrared radiation is given in [3].

2.4 Directional and temporal variation

Apart from the global long term variation, the solar earth irradiation seen by a spacecraft element also varies through the orbit and from orbit to orbit, and with the direction in which the element is pointing. This is both due to the varying relative positions of the Sun, Earth and spacecraft, and due to the kinematics of the spacecraft itself. To get the actual incident irradiation seen by a spacecraft element, the shading by other elements also has to be taken into account. For this a geometrical model of the Proba3 spacecraft is needed, which can simulate the pointing in the orbit and the eventual kinematics of the spacecraft.

2.5 Solar and geomagnetic indices

Solar and geomagnetic indices are used to describe the activity levels of the sun and the disturbance of the geomagnetic field. Most activity indices are given for short periods and as long duration averages. They are also used for long range predictions of solar activities. Many space environment models require activity index values as input parameters.

2.5.1 SOLAR ACTIVITY INDICES

The most frequently used solar activity indices are the sunspot number, R, and the 10.7 cm wavelength radio flux, $F_{10.7}$. These values, which can be measured at the ground, were found to have a strong correlation with the UV radiation of the sun, which has a strong influence on the Earth atmosphere.

The $F_{10.7}$ solar activity index gives the flux at a wavelength of 10.7 cm in units of 10^{-22} W m^{-2} Hz^{-1} also referred to as solar flux units (sfu).

The $F_{10.7}$ index and the sunspot number, R, are correlated. Averaged (over one month or longer) values can be converted by the following expression:

$$F_{10.7} = 63.7 + 0.728\ R + 8.9\ 10^{-4}\ R^2.$$

2.5.2 GEOMAGNETIC ACTIVITY INDICES

Geomagnetic activity indices are used to describe fluctuations of the geomagnetic field. Most widely used planetary indices are K_p and a_p. They are based on 3-hour measurements from 12 ground stations. Values of a_p range from 0 to 400 and they are expressed in units of 2 nanoTesla.

K_p is essentially the logarithm of a_p. The conversion from K_p to a_p is given in Table 2. A daily index, A_p, is obtained by averaging the eight values of a_p for each day.

Table 2: Conversion from K_p to a_p.

K_p	0	0+	1-	10	1+	2-	20	2+	3-	30	3+	4-	40	4+
a_p	0	2	3	4	5	6	7	9	12	15	18	22	27	32

K_p	5-	50	5+	6-	60	6+	7-	70	7+	8-	80	8+	9-	90
a_p	39	48	56	67	80	94	111	132	154	179	207	236	300	400

2.5.3 SOLAR CYCLE DEPENDENCE

The indices $F_{10.7}$ and A_p varies throughout the 11-year solar cycle. The reference index values in table 3 for low, mean and high solar and geomagnetic activities shall be used. The long-term values apply for monthly mean or longer term averaged values. They shall also be used for periods between 1 day and 1 month.

The short duration high values apply for periods of 1 day or less. They shall be used to assess the maximum short-term variations of environmental properties (e.g. atmospheric density fluctuations). Figure 2 and 3 shows the standard prediction of solar and geomagnetic activity indices during a solar cycle.

Table 4 shows when the maximum and minimum solar activity is expected for the next three solar cycles. Some historical data on the variability of these can be found in [5a]. Regular updates of measured and predicted activity values are provided by the Marshall Space Flight Center [5a] and the National Geophysical Data Center [5b]. Indices are also available via the world-wide web via:

http://www.ngdc.noaa.gov/

Table 3: Reference index values

	Long-term (27+days)			Short-duration (daily)		
	Low	**Mean**	**High**	**Low**	**Mean**	**High**
$F_{10.7}$	65	140	250	65	140	300
A_p	0	15	45	0	15	240

Table 4: Solar Cycles

Solar Cycle	**23**	**24**	**25**
Sunspot Minimum	1996.3	2007.3	2018.3
Sunspot Maximum	2000.3	2011.3	2022.3

For use with trapped radiation models as well as for solar particle models described in chapter 4, a period of solar maximum activity is considered to be starting 2.5 years before the year of maximum sunspot number and ending 4.5 years after.

For design purposes the worst case activity values shall be used. These could be the high or low values, depending on the effect to be studied.

2.5.4 GEOMAGNETIC CO-ORDINATES - *B* AND *L*

McIlwain's geomagnetic co-ordinates (or just geomagnetic co-ordinates) *L* and B/B_0, are useful for a number of applications where charged particle morphology or behaviour needs to be described in the magnetosphere. *L* is the radial distance of the field line from the axis at the geomagnetic equator in an ideal dipole field and B is the magnetic field strength, determining the position along a field line from the minimum B_0 at the geomagnetic equator. For many applications the pair *B, L* (or equivalently, B/B_0, *L*) is sufficient to define a location in the field, because of its azimuthal symmetry and the azimuthal symmetry in particle populations. The most important application is in models of the Earth's radiation-belt environment. These particle models give fluxes of trapped energetic particles as functions of particle energy and of geomagnetic co-ordinates *L* and B/B_0.

2.6 Figures

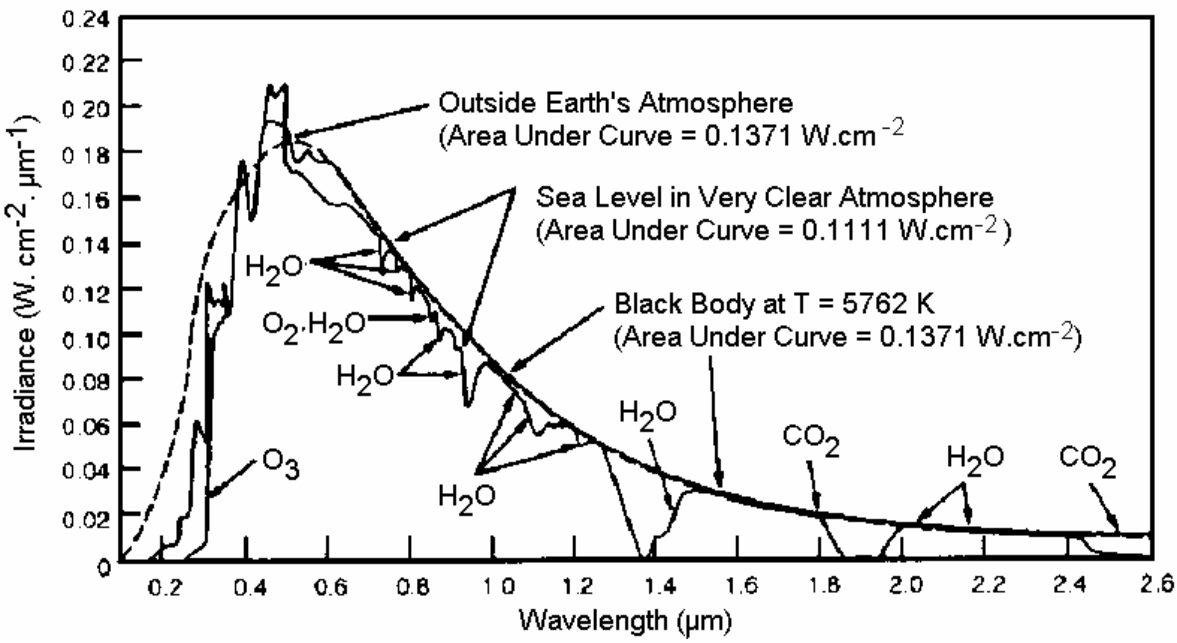

Figure 1: Normally incident solar radiation at sea level on very clear days, solar spectral irradiance outside the Earth's atmosphere at 1 AU, and black body spectral irradiance curve at T=5762 K.

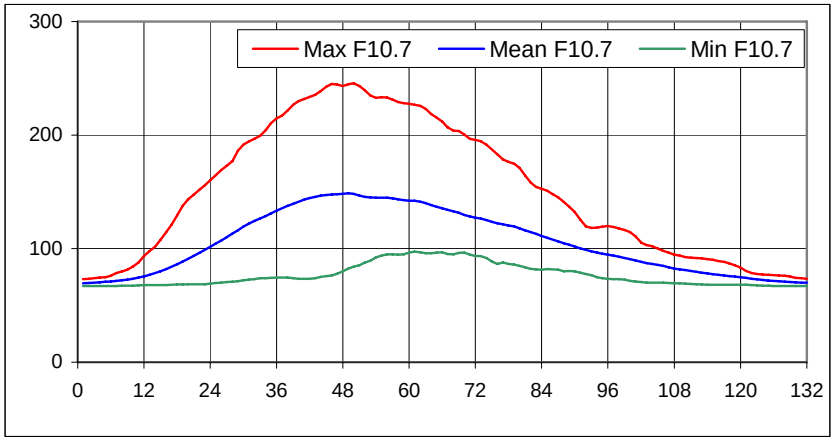

Figure 2: Standard predictions of the F10.7 index during a solar cycle.

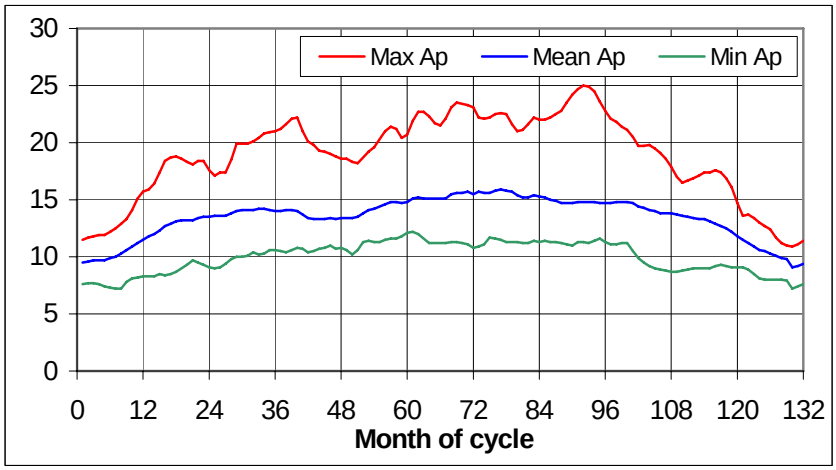

Figure 3: Standard predictions of the Ap index during a solar cycle.

2.7 References

[1] "Natural Orbital Environment Guidelines for Use in Aerospace Vehicle Development", B.J.Anderson, editor and R.E. Smith, compiler; NASA TM 4527, chapters 6 and 9, June 1994

[2] World Meteorological Organization, Compiler: 'Atmospheric Ozone 1985, Assessment of Our Understanding of the Processes Controlling Its Present Distribution and Change', World Meteorological Organization Report, No. 16, Vol.1 Chapter 7, 1985.

[3] "Natural Orbital Environment Guidelines for Use in Aerospace Vehicle Development", B.J.Anderson, editor and R.E. Smith, compiler; NASA TM 4527, chapters 6 and 9, June 1994.

[4] 'Standard Solar Constant and Air Mass Zero Solar Spectral Irradiance Tables', American Society for Testing and Materials, ASTM standard E 490 - 73a (Reapproved 1992).

[5] a) "Solar Activity Inputs for Upper Atmospheric Models', George C. Marshall Space Flight Center, Updates of measured and predicted activities are distributed monthly.
b) Weekly measurements of solar and geomagnetic activity levels are published by the National Geophysical Data Center, Boulder.

3 PLASMAS

3.1 Introduction

A plasma is a partly or wholly ionised gas whose particles exhibit collective response to magnetic and electric fields. The collective motion is brought about by the electrostatic Coulomb force between charged particles. This causes the particles to rearrange themselves to counteract electric fields within a distance of the order of λ, the Debye length.

$$\lambda = \left(\frac{\varepsilon_0 k T_e}{n e^2} \right)^{1/2}$$

where:

λ is in metres
T_e is electron temperature in K
e is electron charge in C
n is density in m^{-3}
k is the Boltzmann constant
ε_0 is the permittivity of vacuum

On spatial scales larger than λ plasmas are electrically neutral.

Spacecraft in Earth orbit experience a number of distinct plasma regimes. At the top of the atmosphere is the so-called ionosphere, above that the magnetosphere, and surrounding this the solar wind, originating on the Sun and blowing throughout interplanetary space. Of these, the regime of main interest for the Proba3 spacecraft, is the magnetosphere. At perigee Proba3 will also encounter the upper part of the ionosphere.

The magnetosphere is an area dominated by the Earth's magnetic field and bounded by the magnetopause. It can be usefully divided into the rather cold low altitude regime (T_e of the order of 1eV) found in the plasmasphere, and the hot high altitude regime (T_e of the order of 10eV to 10keV). Usually the higher energy plasma is the main concern for space systems.

The principal spacecraft engineering concerns for the Proba3 caused by space plasmas are outlined in Table 1.

Table 1: Main engineering concerns for the Proba3 spacecraft due to space plasmas

System	Problem
High-voltage systems	Power leakage, possible arcing, high spacecraft ground potential, sputtering and secondaries
Communication	Ionospheric disturbance of ground-space communications, propagation delays
General	Surface charging, possible harmful electrostatic discharges
Thin film	Degradation, property change

For more information on plasma effects see [13].

3.2 The Ionosphere

3.2.1 DESCRIPTION

The ionosphere is the ionized plasma in the upper atmosphere, produced by the dissociation of atmospheric atoms. It is generally divided into layers D, E and F1 at low altitudes and F2 at higher altitude. The low altitude layers are significant only during daylight hours. F2 is permanent and the densest, peaking at around 300 km altitude. Immediately above the F2 peak, density falls off nearly exponentially with height. At mid to low latitudes, the density fall-off slows down at higher altitudes as the magnetic field traps plasma to form the plasmasphere. Only F2 is relevant for Proba3.

3.2.2 EFFECTS

For most space applications, it is the electron density which is the most important characteristic, causing surface charging and communication disturbances.

3.2.3 MODELS

Ionospheric plasma characteristics are expressed in the International Reference Ionosphere (IRI) [12]. IRI is an empirical model based on a large volume of ground and space data. IRI describes monthly average conditions but can be updated to time-specific conditions using measured characteristic parameters, e.g., F-peak density and height, if these are available. This model calculates densities, temperatures and composition in the altitude range 50 to 1500 km in the non-auroral ionosphere. The model describes the densities of O^+, H^+, He^+, NO^+, O_2^+, N^+, and Cluster ions. External drivers for the IRI model are the sunspot number and the ionospheric index IG; in both cases the 12-month running mean of the index is used.

3.2.4 TYPICAL PARAMETERS

Table 2: Ionospheric Electron density vs. altitude for the IRI-2007 model for date 01/01/2000, lat=0, long=0. Sunspot number Rz12=112

Altitude [km]	Midnight Electron Density (cm^{-3})	Noon Electron Density (cm^{-3})
100	3082	163327
200	16432	231395
300	688694	512842
400	978126	1394750
600	254377	554483
800	85766	148940
1000	40847	62731
1200	23989	34545
1400	16047	22291
1600	11693	15898
1800	9038	12123
2000	7288	9689

3.3 The Plasmaphere

3.3.1 DESCRIPTION

The plasmasphere is a region of cold dense plasma originating in the ionosphere and trapped by the Earth's magnetic field.

Two magnetospheric electric fields, the corotation and cross-tail fields, cause particles, spiralling up and down field lines, to undergo drift perpendicular to the magnetic field. At the altitude of the Proba3 spacecraft, the cross-tail field dominates and drift trajectories carry particles sunwards to the magnetopause, where they are lost from the magnetosphere. The boundary between closed and open drift paths is highly variable and the outer regions of the plasmasphere are continually being lost and refilled over a period of days. Typically, the plasmapause, the outer edge of the plasmasphere, lies at an L-shell of 3 to 6, with a bulge in the dusk region of magnetic local time (MLT).

3.3.2 EFFECTS

Because the plasmasphere contains a dense plasma, it contributes to the radio propagation effects that affect ground-space communications with satellites at high altitude. However densities here are far below ionospheric density, so the effect is not large.

Plasmaspheric ions play a moderating role in spacecraft charging because any strong negative potential attracts ions and is neutralised. Effectively, hazardous surface charging can be said not to occur in the plasmasphere.

3.3.3 MODELS

Because the plasmasphere is quite variable and yet in general does not present major engineering concerns, it has not been considered necessary to define a standard model for this region. Nevertheless, where a model is required for scoping studies of typical plasmasphere parameters, the empirical model of Carpenter and Anderson [1] is recommended. For further information on using this model see [11].

3.3.4 TYPICAL PARAMETERS

Table 2: Electron density vs. L-shell for the Carpenter and Anderson [1] model, ignoring seasonal and solar cycle effects.

L-Shell (Earth radii)	Electron Density (cm^{-3})
4.0	442
4.5	308
5.0	214

Typical ion and electron temperatures, throughout the plasmasphere are of the order of 1eV and 0.5eV respectively. The electron temperature is thus far too low to produce high level charging effects.

3.4 The Outer Magnetosphere

3.4.1 DESCRIPTION

Beyond the plasmapause and within the magnetopause, the magnetospheric plasma environment is characterised by high temperatures and low densities. It drift sunwards from the tail to the near-earth region under the influence of the cross-tail electric field. Some solar wind plasma may enter on the dayside in the cusp or when the solar wind and terrestrial magnetic field merge in a process called reconnection. As plasma moves sunwards from the tail, it is heated adiabatically because it moves to regions of higher magnetic field strength and onto shorter magnetic field lines. In addition, sudden reconnection events in the tail can transfer large amounts of magnetic energy to the plasma which is injected into the near-Earth region. These active periods are called substorms and are detectable on the ground as magnetic disturbances. Hence there is a strong link between

hot plasma and high K_p and AE (Auroral Electrojet) indices. The injected plasma drifts from the region around midnight MLT, westwards (towards dusk) for the ions and eastwards (towards dawn) for the electrons.

Like the plasmapause, the magnetopause is a dynamic boundary. Its location is controlled by the balance between the ram pressure of the flowing solar wind and the magnetic pressure of the terrestrial magnetic field. Along the Earth-Sun line, the magnetopause is closest to the Earth and its forefront position can be expressed approximately [2] as:

$$L_m = \left(\frac{B_0^2}{\mu_0 n m V^2} \right)^{1/6}$$

where:

L_m is the distance from the centre of the Earth to the magnetopause, at the subsolar point, in Earth radii

B_0 is the strength of the terrestrial internal magnetic field, at surface of the earth, on the equator equal to 3×10^4 nT

μ_0 is the permeability of free space

n is the density of the solar wind

m is the mass of the proton

V is the velocity of the solar wind

L_m is typically $10 R_e$ away from the subsolar point, the magnetopause flares out on the flanks and is effectively infinite in length in the anti-solar direction.

3.4.2 EFFECTS

Magnetospheric electrons accumulate on exposed spacecraft surfaces, causing a net current which makes the surface charge negatively. Opposing currents exist which usually prevent significant charging levels, but if these are not sufficient, the spacecraft may charge to hundreds or thousands of volts. Different spacecraft surfaces may charge to different levels and so the possibility of damaging electrostatic discharges exists. Because the intense, high-temperature electrons produced in substorms are usually required, conditions conducive to hazardous charging levels occur mainly in the midnight to dawn quadrant of local time and preferentially around the equinoxes. The regularity with which a spacecraft experiences charging depends on its electrical, geometrical and surface composition characteristics. For the geostationary ATS-5 and -6 satellites, the probability of charging to greater than -10kV during one pass from 00 to 06 LT was between 6% and 12% [3].

Internal, or deep dielectric charging, is discussed in Chapter 4 since it is due to more energetic electrons not normally considered as part of the plasma population.

3.4.3 MODELS

The injection of heated plasma during substorms makes the outer magnetosphere highly dynamic. There are no standard models to describe this region and the standard approach for most engineering purposes is to use worst-case environments.

Garret and DeForest 1979 [4] created a comprehensive model of electron and ion and electron plasma parameters for geostationary orbit. This is not a true empirical model because the source data were selected from periods of frequent substorm injection events but is useful for charging simulations. The model provides bi-Maxwellian descriptions of ions and electron distributions versus magnetic local time and A_p. This representation is convenient for input to a spacecraft charging code such as NASCAP [5].

The single Maxwellian distribution is:

$$f(v) = 4\pi n\left(\frac{m}{2\pi kT}\right)^{3/2} v^2 \exp(-v^2 m / 2kT)$$

where:

n is density

v is velocity

k is Boltzmann's constant

T is temperature

3.4.4 TYPICAL AND WORST CASE PARAMETERS

Typical worst case parameters at the Proba3 orbit are expected to be close to the ones at geostationary orbit. Table 3 gives typical plasma parameters for the Proba3 environment for quiet and substorm periods.

Table 3: Typical plasma parameters at the Proba3 orbit.

	Density (cm^{-3})	**Ion Temperature**	**Electron Temperature**	**λ (m)**
Quiet	10	1eV-1keV	1eV-1keV	50
Substorm	1	10keV	10keV	500

For assessment of surface charging, the following worst-case environment shall be used with the NASCAP [5] charging code or an equivalent code or calculations, applicable to the high altitude environment. It shall apply for all altitudes between the plasmapause and the magnetopause, i.e. between about L=4 R_e and L=10 R_e. This is listed in Table 4. This is a double-Maxwellian fit to an extremely severe event observed by the SCATHA spacecraft on 24 April 1979 [6], when the spacecraft charged to -8kV in sunlight. It should be noted that although the listed ion and electron

densities are not equal, electrical neutrality is maintained by less energetic plasma which is not involved in the charging process and so not listed.

Table 4: Standard worst-case bi-Maxwellian environment.

	Electron Density (cm^{-3})	Electron Temperature (keV)	Ion Density (cm^{-3})	Ion Temperature (keV)
Population 1	0.2	0.4	0.6	0.2
Population 2	1.2	27.5	1.3	28.0

3.5 Induced Environments

The natural plasma environment can be augmented by a number of sources inside or on the satellite surface.

High-energy electron and ion populations can be generated by active experiments, i.e. electron and ion guns. These can be used to control surface charging or as a probe of the magnetic field. An ion thruster is a particularly high-flux ion gun.

Low-energy ion populations can be generated by ionisation (including charge exchange) of contaminant gasses i.e. those released from the Proba3 spacecraft by "outgassing", emitted by thrusters, including ion thrusters and sputtered off the surface due to ion impacts. These contamination processes are described in a separate chapter .

3.5.1 EFFECTS

Once outside the spacecraft, neutral atoms produced by outgassing and sputtering can be ionised by sunlight or charge-exchange with other ions, to create a low-energy (<10eV) ion population. These ions can be drawn to negatively charged surfaces and can adhere. This coating may alter optical properties e.g. of mirrors or solar panel covers, or change the secondary and photoemission yields and the susceptibility to surface charging. Within the spacecraft, e.g. in electronics boxes, residual gasses can facilitate electrostatic discharges from high voltage components.

Photo- and secondary electrons

The electron density at the spacecraft surface shall be determined from the incident UV and primary electron fluxes, multiplied by the yield for the surface in question. Away from the emitting surface the density shall be calculated from the following [7]:

$$\frac{N}{N_0} = (1 + \frac{z}{\sqrt{2}\lambda_0})^{-2}$$

where:

N is density (cm^{-3})

N_0 is density at emitter (cm^{-3})

z is distance from surface

λ_0 is shielding distance, calculated as the Debye length due to the emitted electrons

Once neutral gas is released into space by whatever mechanism, it becomes subject to photoionisation and dissociation by solar UV and ionisation by charge exchange with solar wind ions. Production of new ions can be calculated from the appropriate photoionisation rates and charge exchange cross-sections.

$$Q = N_i(\nu + \sigma n_{sw} v_{sw})$$

from [8] where:

Q is production rate, ions s^{-1}

N_i is ion density

ν is photoionisation rate coefficient

n_{sw} and v_{sw} are solar wind density and velocity

σ is charge exchange coefficient.

Photoionisation rates depends on the atom or molecule concerned, and UV intensity and spectrum. Huebner and Giguere [9] have tabulated a number of rate coefficients for different species, for sunlight at 1AU.

Table 5 gives typical photoelectron sheath parameters [10]:

Table 5: Photoelectron Sheath parameters

Temperature (eV)	Photoelectron current (Amps m^{-2})	Surface electron density (m^{-3})
3	1×10^{-5}	1×10^{8}

3.6 Other effects

3.6.1 IONOSPHERIC PROPAGATION EFFECTS

The most significant propagation effect of the ionosphere is the reflection of waves below a critical frequency, called the plasma frequency, so that communications between ground-stations and spacecraft must take place at higher frequencies. The plasma frequency is a function of electron density, as described below and is typically between 1 and 9 MHz.

$$f_p = \frac{1}{2\pi}\left(\frac{N_e e^2}{\varepsilon_0 m_e}\right)^{1/2} \quad \text{or} \quad f_p = 9N_e^{1/2}$$

where:

f_p is the plasma frequency in s^{-1}

N_e is the electron density in m^{-3}

ε_0 and m_e are natural constants

For high-accuracy positioning of radio beacons by range and/or range rate measurement between a satellite and a ground-based beacon and for radar altimetry, the propagation delay caused by ionospheric plasma density must be considered if distances are to be measured accurately. This delay can be expressed as:

$$\Delta T = -4.03 \text{ X } 10^3 \text{ N / cf}^2$$

where:

ΔT is the propagation delay in seconds

N is electron column density along the path in m^{-2}

c is the velocity of light

f is frequency in s^{-1}

Since the model do not reflect time variations in ionospheric density, altitude corrections for radar altimetry purposes are, in practice, usually made by comparing radio propagation delays at two frequencies. The change in propagation speed of radio waves also means that refraction needs to be considered when calculating satellite orbits by radio tracking.

Below 300MHz degradation of radio signals can occur, principally due to scintillation caused by ionospheric irregularities. Other propagation effects are dispersion, absorption and Faraday rotation.

3.6.2 RAM/WAKE EFFECT

When a spacecraft velocity is higher than or comparable to the ion acoustic velocity, it distorts the plasma environment it experiences, creating a void of particles behind it and often a build-up of particles before it. This effect is seen principally in the ionosphere.

3.6.3 SPUTTERING

Sputtering is the removal of surface material by the impact of ions. Where thin surface coatings are used, this can significantly alter surface characteristics over time and produces a contaminant population which may adhere to other surfaces. This effect is seen principally in the ionosphere.

3.6.4 DOSE EFFECTS ON THIN FILMS

Thin film's properties may be affected by ions with a few tens of keV energy, which can be observed during substorm environment.

3.7 References

[1] Carpenter D.L. and R.R.Anderson, "An ISEE/Whistler Model of Equatorial Electron Density in the Magnetosphere", J.Geophys.Res, 97, p.1097, 1992

[2] Burke W.J., D.A.Hardy and R.P.Vancour, "Magnetospheric and High Latitude Ionospheric Electrodynamics", Chapter 8 of " Handbook of Geophysics and the Space Environment" , Ed. A.Juram, USAF, 1985

[3] Grard R., K. Knott and A. Pedersen, "Spacecraft Charging Effects", Space Science Reviews, 34, p.289, 1983

[4] Garrett H.B. and S.E.DeForest "An Analytical Simulation of the Geosynchronous Plasma Environment", Planet. Space Sci, 27, p.1101, 1979

[5] Katz I., J.J. Cassidy, M.J. Mandell, G.W. Schnuelle, P.G. Steen and J.C. Roche, "The Capabilities of the NASA Charging Analyzer Program", in "Spacecraft Charging Technology -1978", Ed. R.C.Finke and C.P.Pike, NASA CP-2071/AFGL TR-79-0082, ADA045459, p.101, 1979

[6] Gussenhoven M.S and E.G.Mullen, " Geosynchronous Environment for Severe Spacecraft Charging", J.Spacecraft and Rockets 20, p.26, 1988

[7] Grard R.J.L. and J.K.E.Tunaley, "Photo Electron Sheath Near a planar Probe in Interplanetary Space", J. Geophys.Res, 76, p.2498, 1971

[8] Huddleston D.E., A.D.Johnstone and A.J.Coates, "Determination of Comet Halley Gas Emission Characteristics from Mass Loading of the Solar Wind", J.Geophys.Res, 95, p.21, 1990

[9] Huebner W.F. and P.T.Giguere "A Model of Comet Comae II. Effects of Solar Photodissociative Ionization", Astrophys.J, 238, p.753, 1980

[10] Scialdone J.J. "An Estimate of the Outgassing of Space Payloads and Its Gaseous Influence on the Environment", J. Spacecraft and Rockets, 23, p.373, 1986

[11] ECSS-E-ST-10-04C, Space Engineering, Space Environment

[12] Bilitza, D. and B. Reinisch, International Reference Ionosphere 2007: Improvements and New Parameters, Advances in Space Research,, 42, Issue 4, pp. 599-609, 2008.

[13] ECSS-E-20-06, Space Engineering, Spacecraft Charging

4 ENERGETIC PARTICLE RADIATION

4.1 Introduction: Overview of energetic particle radiation environment and effects

Radiation environments and effects are always considered early in the design cycle. Energetic charged particles, which can penetrate outer surfaces of spacecraft (for electrons, this is typically above 100keV, while for protons and other ions this is above 1MeV), are encountered in the orbit of the Proba3 spacecraft, and the effects on both the payload and on the spacecraft carrier have to be considered. Neutrons, gamma-rays and X-rays are also considered energetic particles in this context.

4.1.1 ENVIRONMENTS

Radiation belts

Energetic electrons and ions are magnetically trapped around the earth forming the radiation belts, also known as the Van Allen belts. The radiation belts are crossed by low altitude orbits as well as high altitude orbits (geostationary and beyond). The radiation belts consist principally of electrons of up to a few MeV energy and protons of up to several hundred MeV energy. The so-called south Atlantic anomaly is the inner edge of the inner radiation belt encountered in low altitude orbits. The offset, tilted geomagnetic field brings the inner belt to its lowest altitudes in the south Atlantic region. The Proba3 spacecraft in its highly elliptical orbit continuously traverses the centre of the radiation belts. More information on the radiation belts can be found in references [1] and [2].

Solar energetic particles

Energetic solar eruptions (***solar particle events*** - *SPEs*) produce large fluxes of solar energetic particles (SEPs) which are encountered in interplanetary space and close to the earth. The Earth's magnetic field provides a varying degree of geomagnetic shielding in near-Earth orbits from these particles. The magnitude of these fluxes varies drastically through the 11 years solar cycle. The launch of Proba3 is expected to be in a period of maximum solar activity.

Galactic cosmic-rays

There is a continuous flux of galactic cosmic-ray (GCR) ions. Although the flux is low (a few particles /cm^2/sec), GCRs include energetic heavy ions, which can deposit significant amounts of energy in sensitive volumes and so cause problems.

Secondary radiation

Secondary radiation is generated by the interaction of the above environmental components with materials of the spacecraft. A wide variety of secondary radiations are possible, of varying importance.

4.1.2 EFFECTS SURVEY

The above radiation environments represent important hazards to space missions. Energetic particles, particularly from the radiation belts and from solar particle events cause radiation damage to electronic components, solar cells and materials. They can easily penetrate typical spacecraft walls and deposit considerable doses during a mission.

Energetic ions, primarily from cosmic rays and solar particle events, lose energy rapidly in materials, mainly through ionization. This energy transfer can disrupt or damage targets such as a memory element, leading to single-event upset (SEU) of a component, or an element of a detector (radiation background).

SEUs can also arise from nuclear interactions between very energetic trapped protons and materials (sensitive parts of components, detectors). Here, the proton breaks the nucleus apart and the fragments cause highly-localized ionization.

Energetic electrons can penetrate thin shields and build up static charge in internal dielectric materials such as cable and other insulation, circuit boards, and on ungrounded metallic parts. These can subsequently discharge, generating electromagnetic interference.

Apart from ionizing dose, particles can lose energy through non-ionizing interactions with materials, particularly through “displacement damage”, or “bulk damage”, where atoms are displaced from their original sites. This can alter the electrical, mechanical or optical properties of materials and is an important damage mechanism for electro-optical components (solar cells, opto-couplers, etc.) and for detectors, such as CCDs.

For a more complete description of the effects see [3].

4.2 Quantification of effects and related environments

Models of the radiation environment are needed to assist in orbit selection, component selection and shielding optimization. In engineering a space system to operate in the space environment, it is necessary to relate the environment to system degradation quantitatively. This also involves questions of testing systems and their components for verification that they meet the performance requirements in the presence of the space environment.

For example, testing with calibrated radioactive sources can establish the threshold for functional failure or degradation of an electronic component in terms of *total absorbed dose*. Radiation environment models, used together with mission orbital specifications can predict the dose and enable correct performance to be verified.

The table below gives the parameters, which shall be used for quantification of the various radiation effects.

Table1: Parameters for quantification of radiation effects

Radiation effect	Parameter
Electronic component degradation	Total ionizing dose.
Material degradation	Total ionizing dose.
Material degradation (bulk damage)	Non-ionizing dose (NIEL).
CCD, sensor and opto-electronic component degradation	NIEL
Solar cell degradation	NIEL & equivalent fluence.
Single-event upset, latch-up, etc.	LET spectra (ions); proton energy spectra; explicit SEU/SEL rate of devices.
Sensor interference (background signals)	Flux above above energy threshold and/or flux threshold; explicit background rate.
Internal electrostatic charging	Electron flux and fluence; dielectric E-field.

Although some of these parameters are readily derivable from a specification of the environment, others either need explicit consideration of test data (for example single-event upset calculation) or the detailed consideration of interaction geometry and mechanisms (e.g. radiation background estimation).

In the following sections, the basic data on the environment are presented, along with models to be employed for deriving data beyond those presented. Effects and the specific methods for derivation of engineering quantities will then be presented. Figure 1 shows the ranges of electrons and protons in aluminium.

4.3 Energetic particle radiation environment reference data, models and analysis methods

4.3.1 STANDARD TRAPPED RADIATION BELTS MODELS

For trapped radiation, the standard models of radiation belt energetic particle shall be the AE-8 and AP-8 models for electrons [4] and protons [5] respectively. They were developed at the NSSDC at NASA/GSFC based on data from satellites flown in the '60s and early '70s. The models give omni-directional fluxes as functions of idealized geomagnetic dipole co-ordinates B/B_0 and L . This

means that they must be used together with an orbit generator and geomagnetic field computation to give instantaneous or orbit-averaged fluxes. The user must define an orbit, generate a trajectory, transform it to geomagnetic co-ordinates and access the radiation belt models to compute flux spectra. Apart from separate versions for solar maximum and solar minimum, there is no description of the temporal behaviour of fluxes and no explicit flux directionality. The models shall only be used together with the geomagnetic field models shown in Table 2.

Table-2: Standard field models to be used with radiation-belt models

Radiation-belt Model	**Geomagnetic Field Model**
AE-8-MIN	Jensen-Cain 1960
AE-8-MAX	Jensen-Cain 1960
AP-8-MIN	Jensen-Cain 1960
AP-8-MAX	GSFC 12/66 extrapolated to 1970

The particle ranges shown in figure 1 show that in order to penetrate typical spacecraft shielding of the order of millimetres, protons need tens of MeV energies and electrons need in excess of about 0.5 MeV. The AP-8 model for protons gives proton fluxes from 0.1 to 400 MeV while the AE-8 model for electrons covers electrons from 0.04 to 7 MeV.

Figure 2 and 3 shows the orbit averaged spectra of electrons and protons respectively for the Proba3 orbit as predicted by the AE-8-MAX and AP-8-MAX radiation belt models. It is seen that the fluxes of trapped particles are completely dominated by the electrons. Figure 4 shows the flux of >0.5Mev electrons as a function of time for the Proba3 orbit also as predicted by the AE-8-MAX model. This give an impression of the time variation and the peak values, which can be important if the mission, is sensitive to radiation background in detectors.

It should be remarked that specifically for the geostationary orbit a new model, the IGE 2006 average model [6] (previously called POLE) has been developed. This model has been accepted as new standard model for the Earth radiation belt energetic electrons, but only in this specific orbit.

4.3.2 STANDARD SOLAR PARTICLE EVENT MODEL

During energetic events on the sun, large fluxes of energetic protons are produced which can reach the Earth. Solar particle events, because of their unpredictability and large variability in magnitude, duration and spectral characteristics, have to be treated statistically. However, large events are confined to a 7-year period defined as solar maximum. Although large events are absent during the remaining 4 solar minimum years of the 11-year solar cycle the occasional small event can still occur. The reference model, which shall be used for engineering consideration of time-integrated effects, is the ESP model [7]. This statistical model is based on data from 3 solar cycles. Figure 5 show the predicted spectrum for the Proba3 orbit of solar protons based on this model. In the analysis a solar maximum conditions have been assumed and a confidence level of 95% has been

applied. The ESP model has superseded the JPL-91 model [8], which was a standard for many years, but was shown to underestimate the fluences.

The individual flare spectra are very variable, and what constitutes a worst-case event at one energy is not necessarily worst-case at another. For the higher energies, which are the most important for nuclear interactions giving rise to certain types of background and single-event upsets, the October 1989 event is normally seen as a worst-case. This event produced a peak flux of about 10^5 protons.cm^{-2}.s$^{-1.}$

Geomagnetic Shielding

The Earth's magnetic field partially shields near-earth space orbit from solar energetic particles and cosmic rays, an effect known as geomagnetic shielding. However, these particles still reach polar regions and higher altitudes. Geomagnetic shielding of protons is computed on the basis of the trajectory in geomagnetic B, L space.

At a given location in the field there will be minimum cut-off energies necessary for ions to penetrate to that point. For a quiet magnetosphere the cut-off is excluding protons of about E<200MeV from L<5. However, in reality protons of lower energy can penetrate below L=5 with non-vertical arrival directions, especially in a disturbed magnetosphere where the geomagnetic shielding is weakened. At the L=5 geomagnetic equator in a disturbed magnetosphere, the energy cut-off could be as low 30MeV. Magnetospheric disturbances often follow solar-flares and/or CME's.

Individual Solar particle events

While the standard model provides data only for integrated effects analysis (dose, long-term degradation, total upset count, etc.), it is often necessary to consider individual events. Burrell, as reported in [9], developed a modified Poisson statistic to describe the probability p of a number of events n occurring during a time t, based on a previously observed frequency of N during time T:

$$p(n,t;\, N,T) = \{(n+N)!\ (t/T)^n\} \,/\, \{n!N!\ (1+t/T)^{N+n+1}\}$$

In this equation, N=1 and T=7 for the anomalous class of flare, while for ordinary flares, N=24 and T=7. This is sometimes useful in considering numbers of events in contrast to the total fluence.

Often it is necessary to consider instantaneous fluxes. For radiation background estimation for example, the fluxes are required above an energy threshold determined by sensor shielding and sensor sensitivity, and above a flux threshold determined by sensor signal-to-noise characteristics. Two reference environment data resources are available: NASA OMNIWEB database [10], and the NOAA GOES [11] database. With these databases, the durations and magnitudes of events above energy and flux thresholds can be analysed. Both databases are available on the WWW and provide a comprehensive long-term database of measurements of the interplanetary environment. OMNIWEB contains a complete database of energetic proton data from the IMP series of spacecraft. The NOAA GOES satellites have returned energetic proton and electron data from geostationary orbit since January 1986.

Solar particle event ions

For analysing single event upset rates during solar particle events (SPE's), the CREME96 model shall be used. It can also be used for other applications where data on severe SPE conditions are needed, such as background estimation. CREME96 is described further in [12]. While the older CREME model contained models for the peak flux for various types of events, CREME96 contains models based on the October 1989 event. It provides models of energy spectrum, composition and LET spectrum for the worst week, worst day and peak 5 minutes. The older CREME model provided more choice of peak environments. However, some of the more severe options were unrealistic.

4.3.3 COSMIC RAY ENVIRONMENT AND EFFECTS MODELS

Cosmic-Ray environment and effects models were originally created by Adams and co-workers at the U.S. Naval Research Laboratory [13], under the name CREME. They provided a comprehensive set of cosmic ray and flare ion LET and energy spectra, including treatment of geomagnetic shielding and material shielding. CREME also included upset rate computation based on the path-length distribution in a sensitive volume and also treated in a simple manner trapped proton-induced SEUs. CREME has been superseded by CREME96 [13]. The major differences are in the inclusion of a model of the cosmic ray environment and its solar-cycle modulation due to Nymmik et al. [14], improved geomagnetic shielding calculation, improved material shielding calculation and more realistic solar energetic particle event (SEPE) ion environments. Cosmic ray fluxes are anti-correlated with solar activity so the highest cosmic ray fluxes occur at solar minimum. CREME96 shall be the standard model for cosmic ray environment assessment. It shall also be the standard for evaluation of single event effects from cosmic rays, from solar energetic particles and from energetic protons.

Figure 6 shows composite LET spectra in the Proba3 orbit for three CREME96 environments: the nominal solar minimum cosmic ray flux; the average flux for a "worst week" of a large SEPE; and the peak flux from a large SEPE. Ions from Z=1 to 92 shall be included and, in the absence of a reason to use another value, shielding of $1 g/cm^2$ aluminium shall be assumed.

4.3.4 SPACECRAFT SECONDARY RADIATION

For engineering purposes it is often only electron-induced bremsstrahlung radiation that is considered as a significant secondary source. Bremsstrahlung is high-energy electromagnetic radiation in the X-γ energy range emitted by charged particles slowing down by scattering off atomic nuclei. The primary particle might ultimately be absorbed while the bremsstrahlung can be highly penetrating. In space, the most common source of bremsstrahlung is electron scattering. In special cases other secondaries, such as neutrons or spallation products from nuclear reactions, need to be considered.

In evaluating the radiation background effects in detector systems, it is often secondary radiation that is important. This might be because of heavy shielding removing primaries, veto systems which actively protect against counting primary-induced signals, or secondary radiation generated within the sensing band of an instrument. Most secondary radiation is emitted at the instant of interaction ("prompt") while some is emitted some time after a nucleus has been excited by an incoming particle (induced radioactivity).

By its nature, secondary radiation has to be analysed on a case-by-case basis, possibly through Monte-Carlo simulation. For engineering estimates of bremsstrahlung, the SHIELDOSE model [15] shall be used.

4.4 Analysis methods for derived quantities

The following analysis methods shall be used.

The environment models specified in 4.3 shall be used to generate the primary data described in Section 4.2. The secondary data shall be derived as follows:

4.4.1 IONIZING DOSE

The ionizing dose environment is represented by the dose-depth curve. This may provide dose as a function of shield thickness in planar geometry or as a function of spherical shielding about a point. The planar model is appropriate for surface materials or for locations near to a planar surface. In general, electronic components are not in such locations and a spherical model is recommended for general specification.

The SHIELDOSE model shall be used [15] for ionizing dose. This method uses a pre-computed data-set of doses from electrons, electron-induced bremsstrahlung and protons, as derived from Monte-Carlo analysis. The doses are provided as functions of material shielding thickness. The reference geometrical configuration for this dose-depth curve shall be a solid aluminium sphere. Figures 7 shows the expected accumulated doses for the Proba3 orbit as functions of the radius of the aluminium shielding. It is seen that the dose is dominated by the contribution from electrons. For shielding higher than 7mm Aluminium the trapped protons becomes the most important.

In cases where more careful analysis of the shielding of a component or of other sensitive locations is necessary, a sectoring calculation is performed on the geometry of the system. This might be necessary if the doses computed from simple spherical shielding are incompatible with the specification of the allowable radiation dose. The sectoring method traces rays from the point of interest through the shielding in a large number of directions. Along each direction the derived shielding, together with the data on dose as a function of shielding depth, d, is used to find the omnidirectional 4π dose contribution from each direction. The contributions, weighted by the solid angle increment around the rays, are then summed to give the total dose. In some cases, it is efficient to derive a shielding distribution. This is also the result of the ray-tracing described above and provides the distribution of encountered shielding.

It is important to recognise that a shielding analysis in the presence of significant anisotropies in the environment can result in serious error if the environment is assumed to be isotropic. This assumption is implicit in the sectoring method defined above since all directional contributions are derived from a common "omnidirectional" dose-depth curve.

4.4.2 SINGLE-EVENT UPSET RATE

The CREME/CREME96 method shall be used [12], [13]. It is possible to make upset rate predictions only when details of the device under consideration are known, particularly the critical charge and the sensitive volume dimensions. If a device is uncharacterized, tests shall be performed.

The test data shall show the normalized upset rate as a function of ion LET in the range 1 to 100 MeV.cm^2/mg and as a function of proton energy in the range 20-100MeV. These data shall be used to make an estimate of the upset rate from trapped protons and solar protons using the two-parameter Bendel method [16], and of upsets due to galactic and solar ions using the method of CREME/CREME96. This latter shall be modified to account for the non-ideal upset rate as a function of ion LET derived from component test data [17] (the so-called "IRPP" method) as described below. This method has been implemented in CREME96. CREME96 also includes the two-parameter Bendel method.

To compute an upset rate for an electronic device or a detector from the predicted fluxes, device characteristics must be specified, particularly the size of the sensitive volume and the *critical charge*, or equivalently, critical energy E_c, in the volume which results in upset or registers as a "count". For SEUs resulting from direct ionisation the rate is found by integrating over the composite differential ion LETspectrum and the distribution of path-lengths for the sensitive volume [14], [17]. An estimate of the upset rate from nuclear interactions of energetic protons can be obtained by integration of the product of the measured proton-induced upset cross section $\sigma(E)$ and the differential proton flux$f(E)$ over all energies. $\sigma(E)$ can be derived directly from the test data, or the 2-parameter Bendel fit can be used.

4.4.3 SOLAR CELL DEGRADATION

The EQUFRUX model shall be used for solar cell degradation calculations [18]. In the absence of other test data, it shall be assumed that 10MeV protons cause equivalent damage to 3000 1 MeV electrons in silicon cells. Similarly it shall be assumed for gallium arsenide cells that the damage equivalence of a 10MeV proton is 400, 1000 and 1400 1 MeV electrons for short-circuit current, maximum power and open-circuit voltage degradation respectively. Since the default in these models is the assumption of infinite rear-side shielding of cells, this shall be the standard way of reporting results. However, account shall then be explicitly taken of radiation penetration though the rear-side of solar arrays. Figure 8 show the predicted equivalent 1MeV electron fluence for solar cell degradation for the Proba3 orbit as functions of the cover glass thickness. The data quoted are for Spectrolab 3J cells and end of life predictions. The conversion to damage equivalent fluences is based on damage ratios published in [19]. The data is split in the contribution from protons and electrons respectively.

4.4.4 INTERNAL ELECTROSTATIC CHARGING

Internal electrostatic charging (or deep-dielectric charging) results from the build-up over a longer period of electrostatic charge. Since the Proba3 orbit is continuously passing through the hart of the electron radiation belts it will encounter high levels of energetic electron flux, and it is therefore important to assess whether the spacecraft is liable to experience electrostatic discharges or not. The charge build-up depends on the severity of the environment and the dielectric resisitivity of the susceptible part (or lack of grounding of floating metalisation). The actual discharge may also depend on properties such as geometry and material condition. Charge build-up can therefore be mitigated by choice of material and grounding, but also by employing shielding to reduce the severity of the environment.

Established radiation-belt models, like AE8, are inappropriate for use as input for a model dealing with internal charging, since they represent average conditions, not the disturbed conditions that produce breakdown in dielectrics. Intensity, spectral hardness and duration of the disturbed environment are all factors that must be taken into account for analysis of internal charging.

To address these issues it is recommended to use the FLUMIC model. This model is part of the DICTAT tool [20] [21] which has been incorporated in the Space Environment Information System http:www.spenvis.oma.be/. The model is based on worst-case 1-day fluences using STRV-1b REM data (courtesy of Paul Scherrer Institute, Switzerland) and GOES-7 data (courtesy of NOAA, USA). One day is seen as the appropriate time-scale for internal charging problems. Figure 9 shows the worst-case electron flux for the Proba3 orbit as predicted by the FLUMIC model. For comparison the figure also show the corresponding prediction for the geostationary orbit. The predicted flux varies considerably with the solar cycle and the time of the year. The curves in the figure correspond to a maximum in terms of these variations.

More complex tools are also available which employs a Monte-Carlo radiation transport method to compute the charge build-up in a dielectric material in a certain environment. Other very useful guidelines related to internal charging can be found in [22]

4.4.5 NON-IONIZING DOSE

Damage to CCDs and other electro-optical components susceptible to displacement damage shall employ the NIEL function, N(E) [23], shown in Figure 10, to derive an equivalent proton damage fluence F_D:

$F_D = \Sigma_E f(E).\ N_{10}(E)\ .\ \Delta E$

or a non-ionizing dose, D_N:

$$D_N = \Sigma_E f(E).\ N(E)\ .\ \Delta E$$

where: $f(E)$ is the differential fluence spectrum

$N(E)$ is the NIEL function

$N_{10}(E)$ is the NIEL function normalised to 10MeV

ΔE is the energy step of the sum.

Figure 11 to 13 show the non-ionising energy loss and the equivalent 10MeV, 60MeV and 200MeV proton fluence for the Proba3 orbit. To turn this into a relative degradation (e.g. Charge Transfer Efficiency loss in a CCD) it is necessary to test the specific detector in question to find its response to such an environment.

4.5 Links with radiation testing

The table below recalls the parameter used for quantification of various radiation effects, and for illustration purposes, lists the types of testing which must be done to verify compatibility with the effects. See [24] for further details.

Radiation effect	**Parameter**	**Test means**
Electronic component degradation	Total ionising dose	Radioactive sources (e.g ^{60}Co), particle beams (e^-,p^+)
Material degradation	Total ionising dose	Radioactive sources (e.g ^{60}Co), particle beams (e^-,p^+)
Material degradation (bulk damage)	Non-ionising dose (NIEL)	Proton beams
CCD and sensor degradation	Non-ionising dose (NIEL)	Proton beams
Solar cell degradation	Non-ionising dose (NIEL) & equivalent fluence.	Proton beams (~ low energy)
Single-event upset, Latch-up,etc.	LET spectra (ions), proton energy spectra, explicit SEU/L rate.	Heavy ion particle beams Proton particle beams ⇦
Sensor interference (background signals)	Flux above energy threshold, flux threshold, explicit background rate.	Radioactive sources, particle beams ⇦
Internal electrostatic Charging	Electron flux and fluence dielectric E-field.	Electron beams ⇦ Discharge characterisation

⇦ = test data feed back to calculation

e, p = electron, protons

4.6 Sources of models

Most models mentioned are also installed in the Space Environment Information System (Spenvis). Further information on Spenvis and analysis of space radiation environments and effects can be found on various WWW sites:

ESTEC Space Systems Environment Analysis Site	http://www.estec.esa.nl/wmwww/wma
ESA/BIRA Space Environment Information System	http://www.spenvis.oma.be/spenvis/
NASA Space Environment and Effects Site	http://see.msfc.nasa.gov/

4.7 Figures

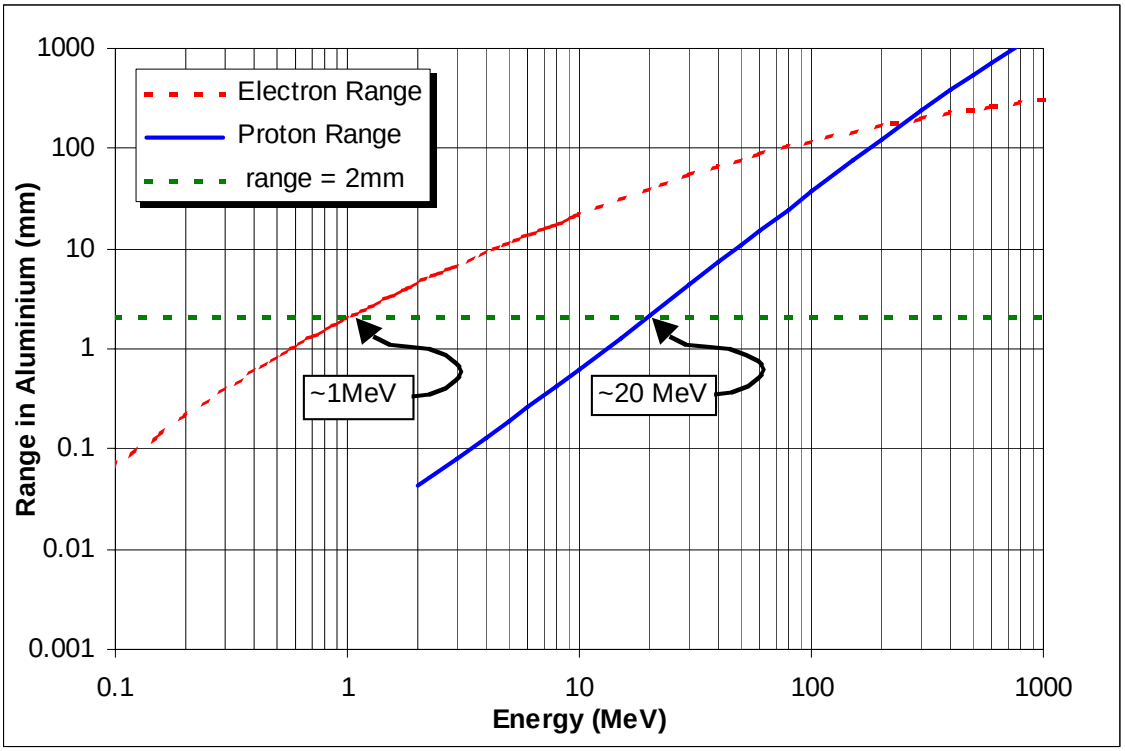

Figure 1: Mean ranges of protons and electrons in aluminium.

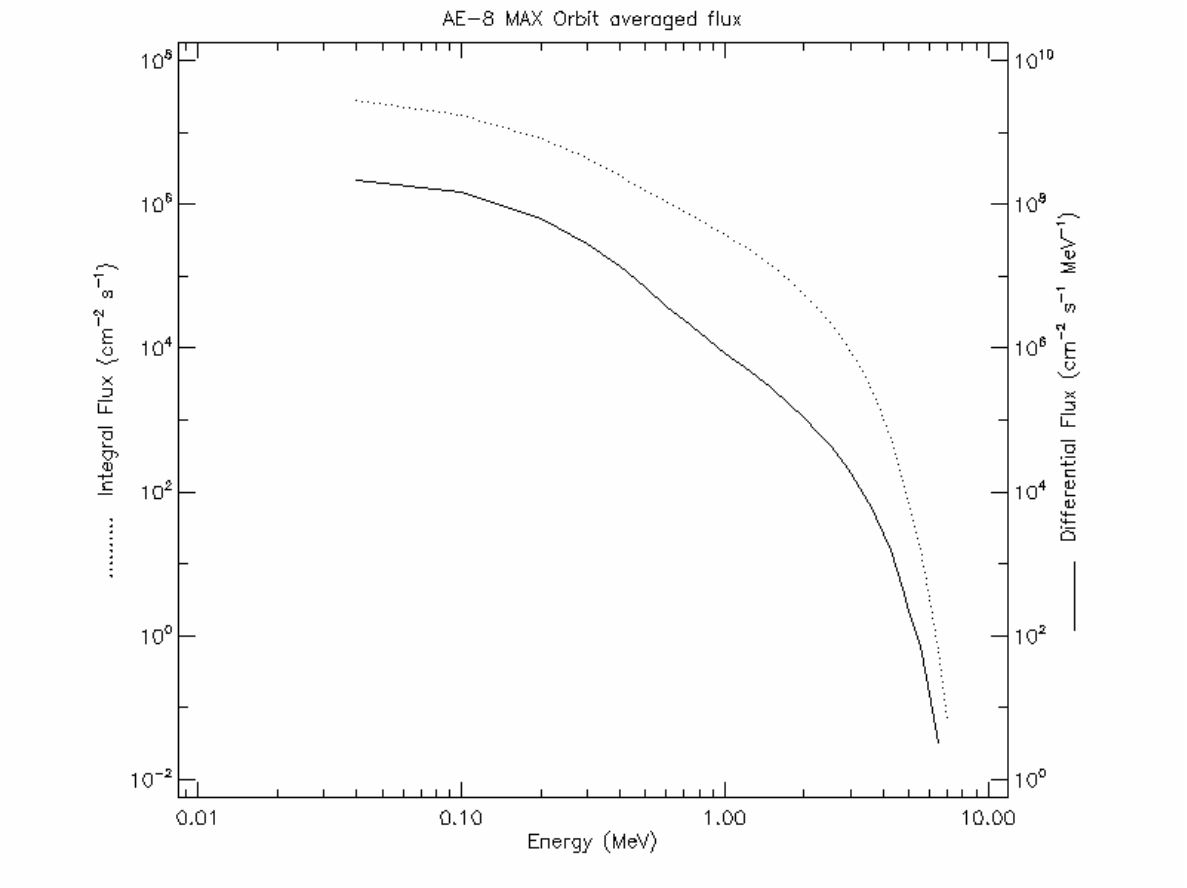

Figure 2: AE-8 orbit averaged trapped electron spectrum for the Proba3 orbit

Energy [MeV]	Integral Flux [/cm2/s]
0.04	2.82E+07
0.1	1.71E+07
0.2	8.21E+06
0.3	4.32E+06
0.4	2.53E+06
0.5	1.56E+06
0.6	1.09E+06
0.7	7.82E+05
0.8	5.95E+05
1	3.81E+05
1.25	2.32E+05
1.5	1.43E+05
1.75	9.02E+04
2	5.70E+04
2.25	3.64E+04
2.5	2.34E+04
2.75	1.44E+04
3	8.88E+03
3.25	5.39E+03
3.5	3.29E+03
3.75	1.86E+03
4	1.06E+03
4.25	5.60E+02
4.5	2.99E+02
4.75	1.43E+02
5	7.26E+01
5.5	1.61E+01
6	3.34E+00
6.5	6.06E-01
7	6.90E-02

Figure 2 (continued): AE-8 orbit averaged trapped electron spectrum for the Proba3 orbit

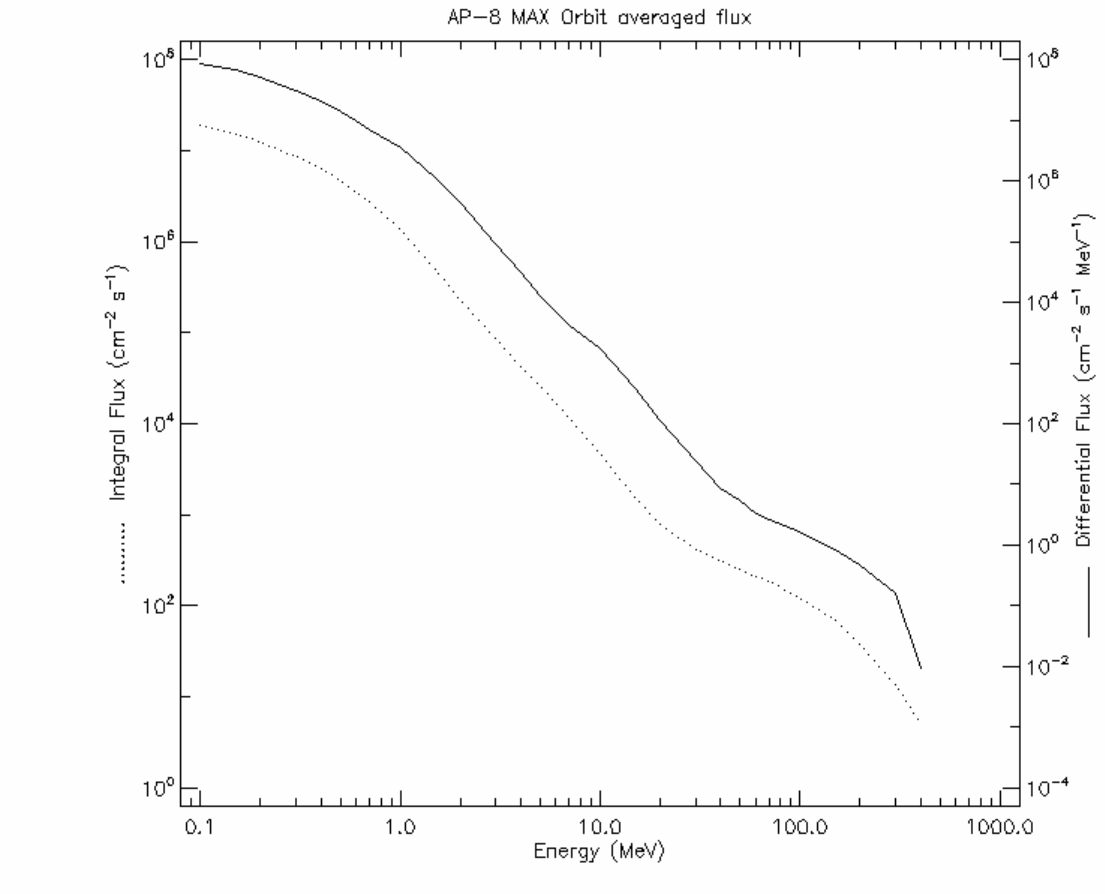

Figure 3: AP-8 orbit averaged trapped proton spectrum for the Proba3 orbit

Energy [MeV]	Integral Flux [/cm2/s]
0.1	1.90E+07
0.15	1.52E+07
0.2	1.23E+07
0.3	8.66E+06
0.4	6.21E+06
0.5	4.62E+06
0.6	3.49E+06
0.7	2.70E+06
1	1.33E+06
1.5	5.02E+05
2	2.22E+05
3	8.77E+04
4	4.25E+04
5	2.60E+04
6	1.67E+04
7	1.17E+04
10	4.70E+03
15	1.55E+03
20	8.02E+02
30	4.20E+02
40	3.19E+02
50	2.49E+02
60	2.12E+02
70	1.85E+02
100	1.24E+02
150	6.83E+01
200	3.79E+01
300	1.37E+01
400	5.02E+00

Figure 3 (continued): AP-8 orbit averaged trapped proton spectrum for the Proba3 orbit

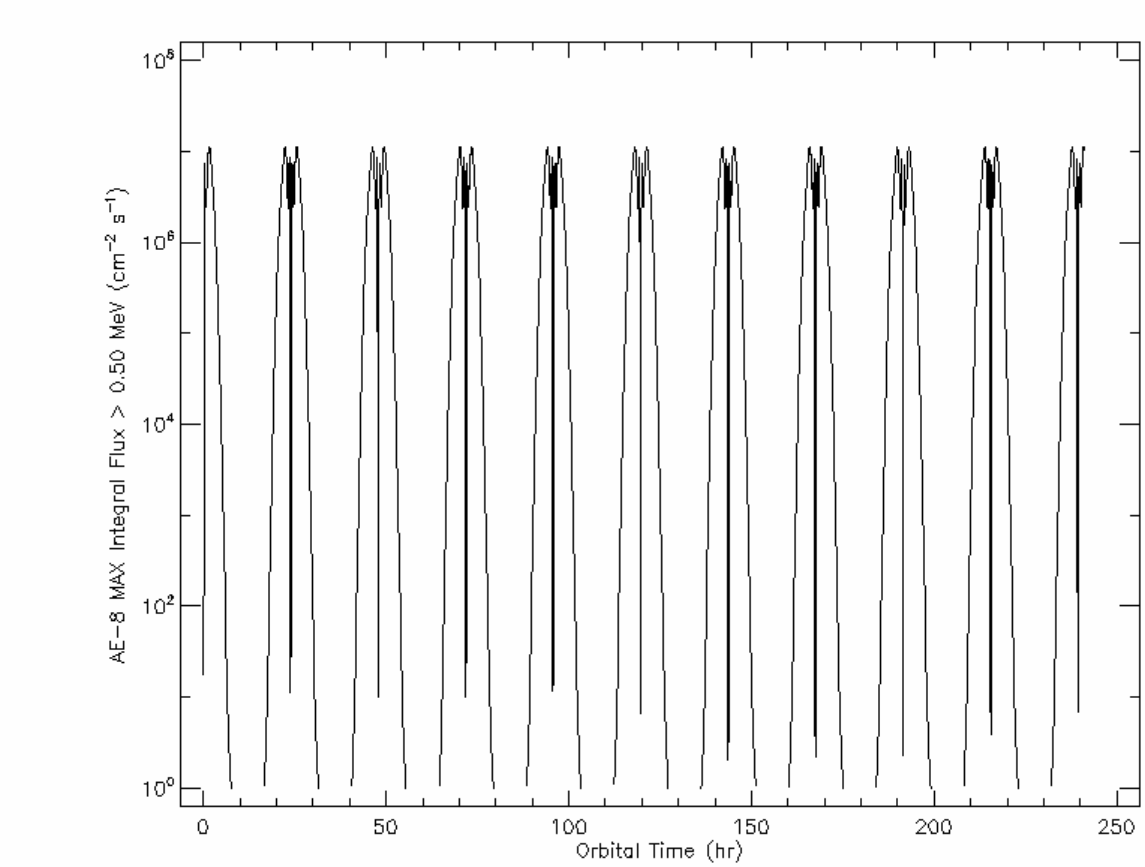

Figure 4: AE-8-MAX trapped flux of >0.5MeV electrons as a function of time for the Proba3 orbit

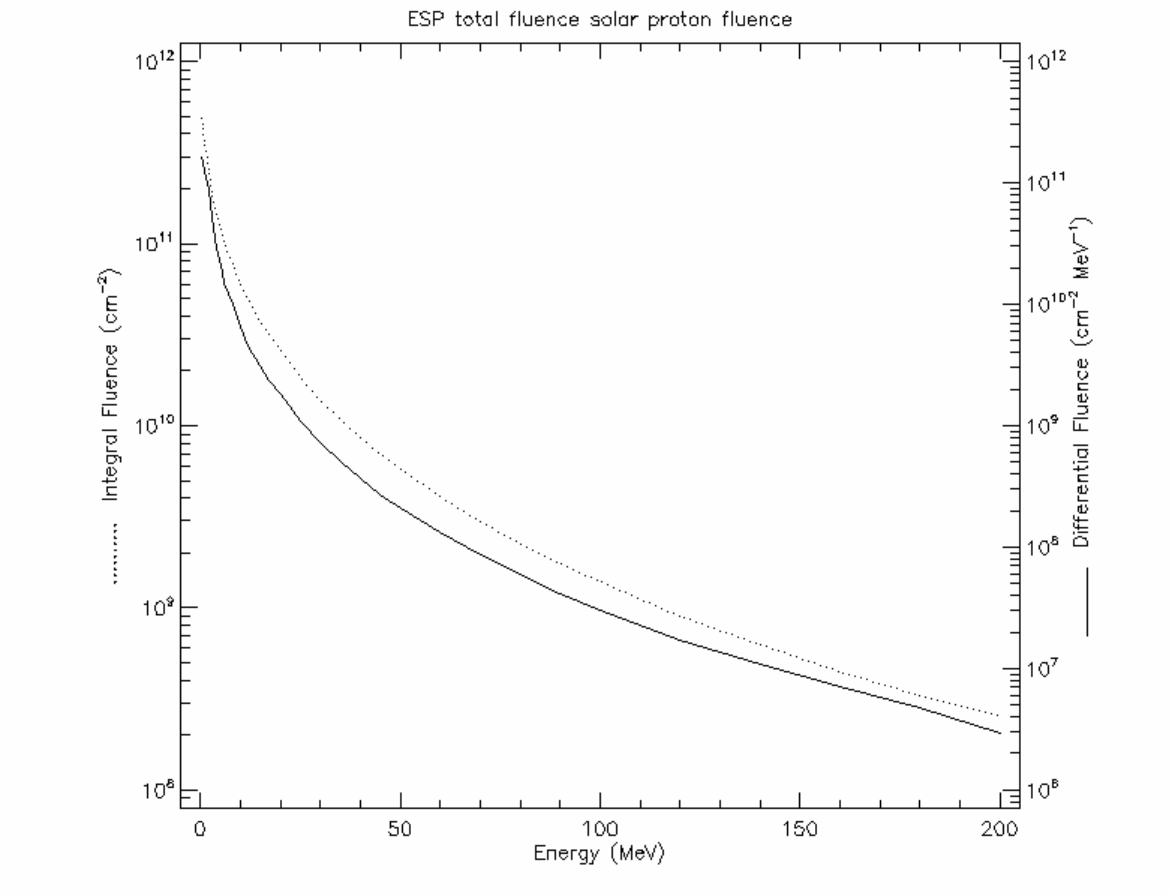

Figure 5: Solar proton spectrum for the Proba3 orbit (duration 2 years, data from ESP model)

Energy [MeV]	Integral Fluence [/cm2]
0.1	4.90E+11
0.5	4.20E+11
1	3.60E+11
2	2.50E+11
3	1.80E+11
4	1.40E+11
5	1.20E+11
6	1.00E+11
8	7.60E+10
10	6.00E+10
12	4.90E+10
15	3.70E+10
17	3.20E+10
20	2.60E+10
25	1.80E+10
30	1.40E+10
35	1.10E+10
40	8.60E+09
45	7.00E+09
50	5.80E+09
60	4.10E+09
70	3.00E+09
80	2.30E+09
90	1.70E+09
100	1.40E+09
120	9.00E+08
140	6.20E+08
160	4.40E+08
180	3.30E+08
200	2.50E+08

Figure 5 (continued): Solar proton spectrum for the Proba3 orbit (duration 2 years, data from ESP model)

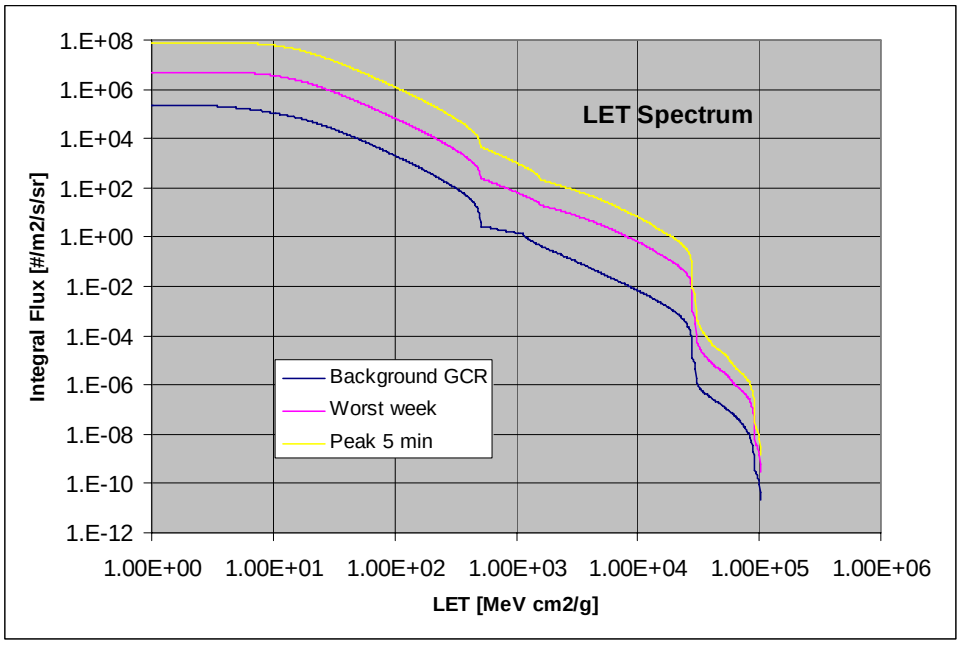

LET Spectrum			
	Integral Flux [#/m2/s/sr]		
LET [MeV cm2/g]	Background GCR	Worst Week	Peak 5 Min
1.E+00	2.24E+05	5.02E+06	7.79E+07
3.E+00	2.11E+05	4.98E+06	7.76E+07
6.E+00	1.58E+05	4.57E+06	7.33E+07
1.E+01	1.10E+05	3.62E+06	6.06E+07
3.E+01	2.65E+04	8.57E+05	1.55E+07
6.E+01	6.52E+03	2.10E+05	3.86E+06
1.E+02	2.01E+03	6.61E+04	1.22E+06
3.E+02	1.15E+02	4.03E+03	7.50E+04
6.E+02	2.39E+00	1.80E+02	3.23E+03
1.E+03	1.48E+00	6.61E+01	1.05E+03
3.E+03	1.11E-01	7.88E+00	8.10E+01
6.E+03	2.28E-02	2.15E+00	2.23E+01
1.E+04	6.69E-03	6.34E-01	6.39E+00
3.E+04	4.62E-06	2.98E-04	2.76E-03
6.E+04	6.73E-08	1.32E-06	6.87E-06
1.E+05	2.06E-11	2.94E-10	1.44E-09

Figure 6: Cosmic ray LET spectra for the Proba3 orbit as calculated by CREME96

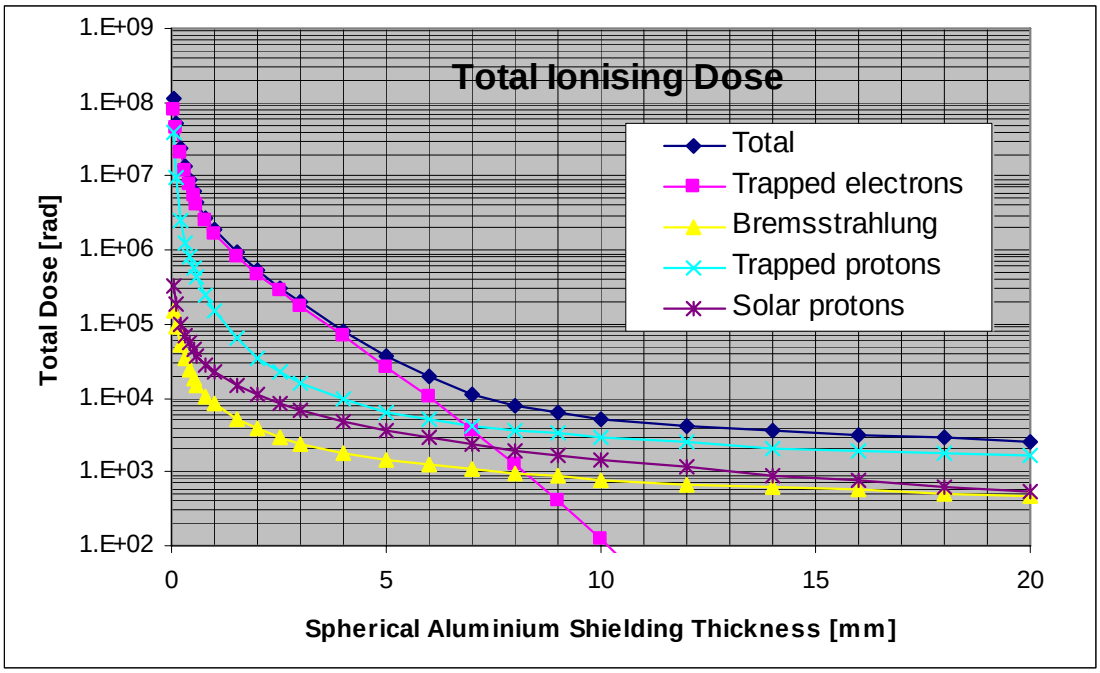

Figure 7: Dose-Depth Curve for the Proba3 orbit (2 years)

Shielding Thickness [mm]	Total ionising dose in Si for Spherical Al Shielding [rad]				
	Total	Electrons	Brems-strahlung	Trapped Protons	Solar Protons
0.05	1.16E+08	7.83E+07	1.51E+05	3.84E+07	3.38E+05
0.1	5.28E+07	4.37E+07	9.31E+04	9.28E+06	1.83E+05
0.2	2.35E+07	2.11E+07	5.18E+04	2.48E+06	1.00E+05
0.3	1.35E+07	1.23E+07	3.40E+04	1.26E+06	7.20E+04
0.4	8.77E+06	7.94E+06	2.44E+04	8.06E+05	5.58E+04
0.5	6.12E+06	5.51E+06	1.87E+04	5.73E+05	4.51E+04
0.6	4.49E+06	4.04E+06	1.51E+04	4.24E+05	3.76E+04
0.8	2.74E+06	2.47E+06	1.07E+04	2.45E+05	2.83E+04
1	1.87E+06	1.69E+06	8.34E+03	1.54E+05	2.28E+04
1.5	9.16E+05	8.39E+05	5.30E+03	6.34E+04	1.51E+04
2	5.21E+05	4.77E+05	3.83E+03	3.40E+04	1.11E+04
2.5	3.15E+05	2.85E+05	2.97E+03	2.21E+04	8.58E+03
3	1.97E+05	1.74E+05	2.44E+03	1.58E+04	6.87E+03
4	8.28E+04	6.78E+04	1.80E+03	9.47E+03	4.83E+03
5	3.76E+04	2.66E+04	1.44E+03	6.53E+03	3.62E+03
6	1.91E+04	1.01E+04	1.22E+03	5.10E+03	2.90E+03
7	1.12E+04	3.67E+03	1.06E+03	4.25E+03	2.36E+03
8	7.80E+03	1.25E+03	9.44E+02	3.71E+03	1.98E+03
9	6.23E+03	4.02E+02	8.58E+02	3.33E+03	1.70E+03
10	5.31E+03	1.21E+02	7.90E+02	2.98E+03	1.47E+03
12	4.28E+03	8.98E+00	6.90E+02	2.47E+03	1.15E+03
14	3.63E+03	2.80E-01	6.19E+02	2.13E+03	9.12E+02
16	3.20E+03	2.14E-03	5.65E+02	1.92E+03	7.48E+02
18	2.90E+03	2.55E-05	5.20E+02	1.78E+03	6.31E+02
20	2.62E+03	0.00E+00	4.78E+02	1.64E+03	5.30E+02

Figure 7 (continued): Dose-Depth Curve for the Proba3 orbit (2 years)

Solar cells equivalent 1MeV electron fluence
for Spectrolab 3J EOL cells
(Electron/proton damage ratios: Pmax: 870.0, Voc: 1020.0, Isc: 565.0)

Cover Glass Thickness (Microns)	Total		
	Pmax [#/cm2]	Voc [#/cm2]	Isc [#/cm2]
0	4.72E+18	5.54E+18	6.56E+18
25.41	6.05E+16	7.09E+16	6.88E+16
76.36	6.65E+15	7.80E+15	6.43E+15
152.27	1.80E+15	2.10E+15	1.60E+15
305	5.38E+14	6.28E+14	4.48E+14
509.09	2.12E+14	2.46E+14	1.73E+14
761.36	9.50E+13	1.10E+14	6.80E+13
1522.73	3.32E+13	3.83E+13	2.22E+13

Cover Glass Thickness (Microns)	Trapped Electrons		
	Pmax [#/cm2]	Voc [#/cm2]	Isc [#/cm2]
0	4.57E+13	4.57E+13	4.57E+13
25.41	3.91E+13	3.91E+13	3.91E+13
76.36	3.22E+13	3.22E+13	3.22E+13
152.27	2.59E+13	2.59E+13	2.59E+13
305	1.85E+13	1.85E+13	1.85E+13
509.09	1.31E+13	1.31E+13	1.31E+13
761.36	9.26E+12	9.26E+12	9.26E+12
1522.73	4.04E+12	4.04E+12	4.04E+12

Cover Glass Thickness (Microns)	Trapped Protons		
	Pmax [#/cm2]	Voc [#/cm2]	Isc [#/cm2]
0	4.83E+18	5.66E+18	6.70E+18
25.41	6.17E+16	7.23E+16	7.02E+16
76.36	6.63E+15	7.77E+15	6.42E+15
152.27	1.73E+15	2.03E+15	1.55E+15
305	4.87E+14	5.71E+14	4.07E+14
509.09	1.77E+14	2.07E+14	1.44E+14
761.36	7.08E+13	8.30E+13	4.93E+13
1522.73	2.09E+13	2.45E+13	1.32E+13

Cover Glass Thickness (Microns)	Solar Protons		
	Pmax [#/cm2]	Voc [#/cm2]	Isc [#/cm2]
0	9.62E+14	1.13E+15	1.06E+15
25.41	3.29E+14	3.86E+14	3.10E+14
76.36	1.44E+14	1.68E+14	1.23E+14
152.27	7.71E+13	9.04E+13	6.11E+13
305	4.16E+13	4.88E+13	3.07E+13
509.09	2.52E+13	2.96E+13	1.79E+13
761.36	1.62E+13	1.90E+13	1.03E+13
1522.73	8.65E+12	1.01E+13	5.19E+12

Figure 8: Solar cell equivalent 1MeV electron fluences for the the Proba3 orbit

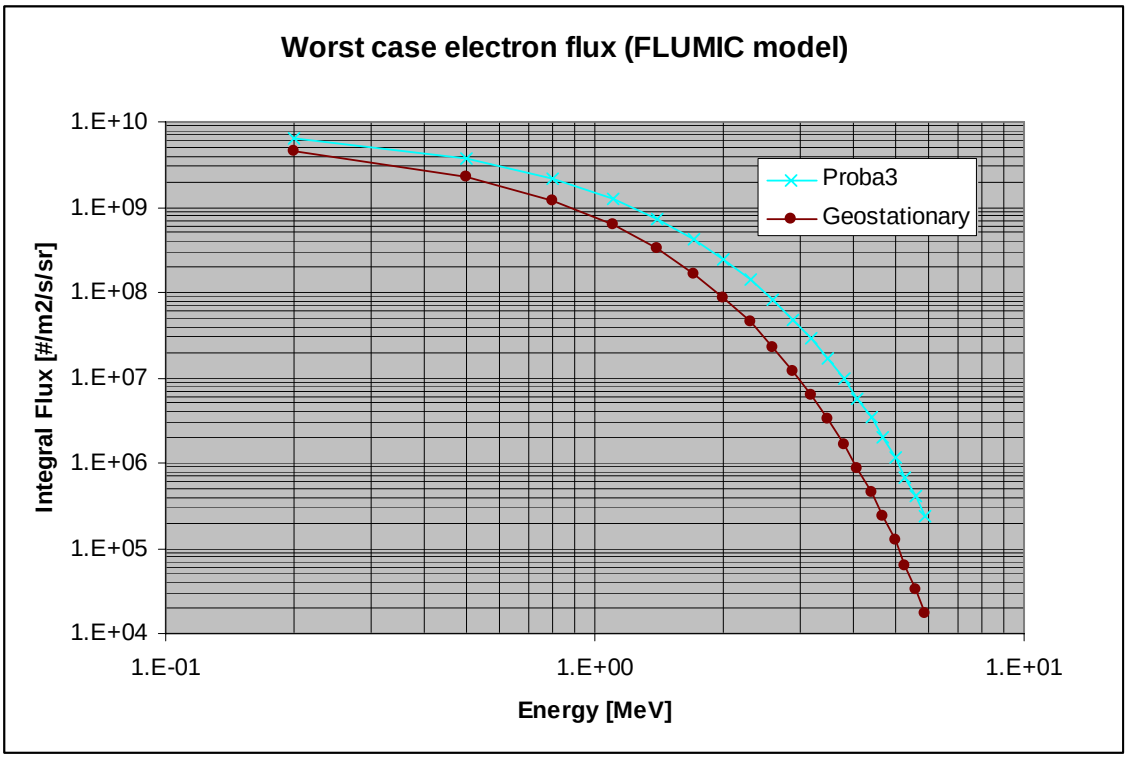

Figure 9: Worst case electron flux for the Proba3 orbit
for assessment of internal charging (FLUMIC model)

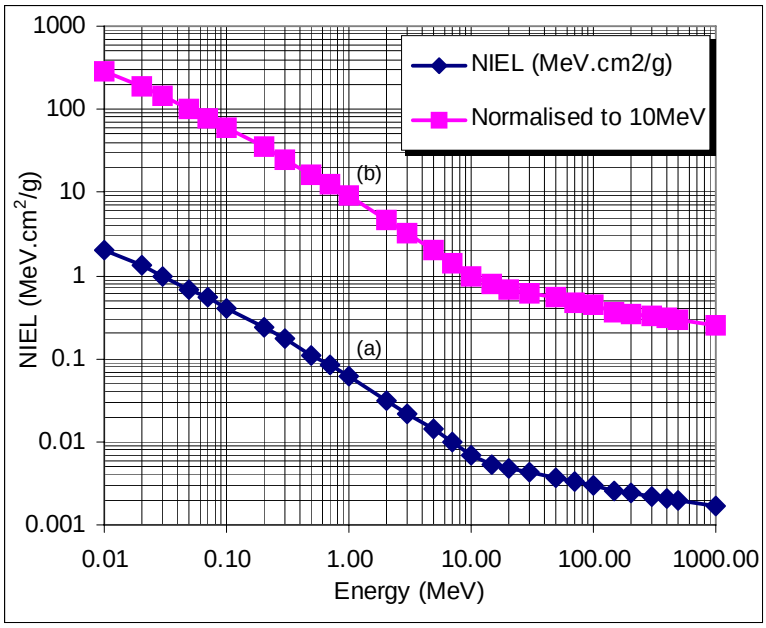

Figure 10: NIEL curve: (a) energy lost by protons in non-ionizing interactions (bulk, displacement damage); (b) NIEL relative to 10MeV giving damage-equivalence of other energies.

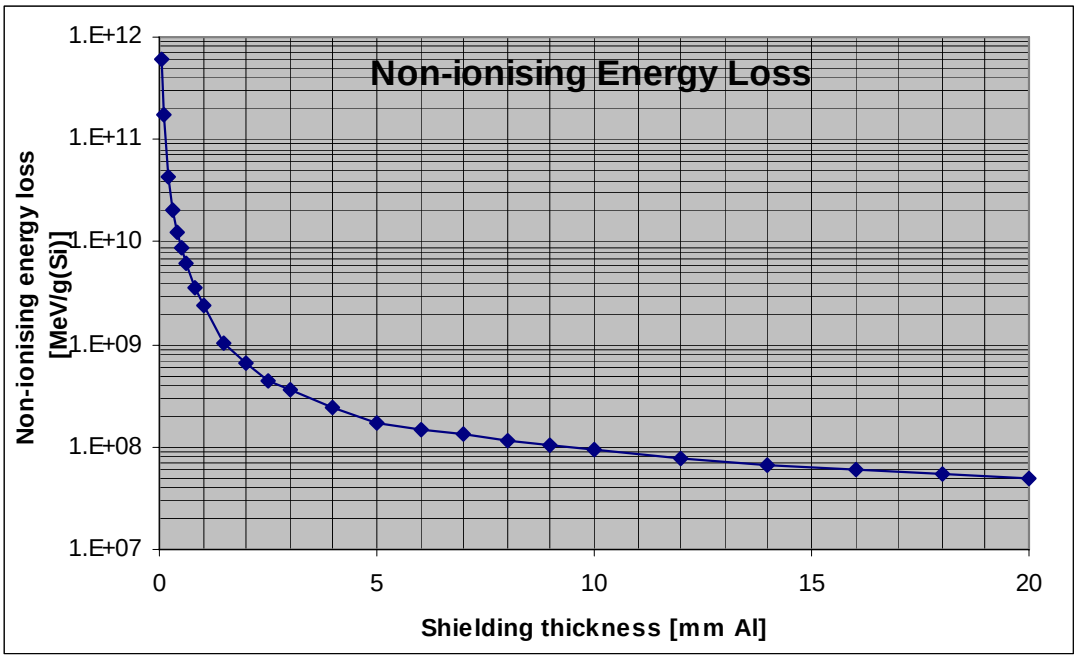

Figure 11: Non-ionising energy loss as a function of Al shielding for the Proba3 orbit

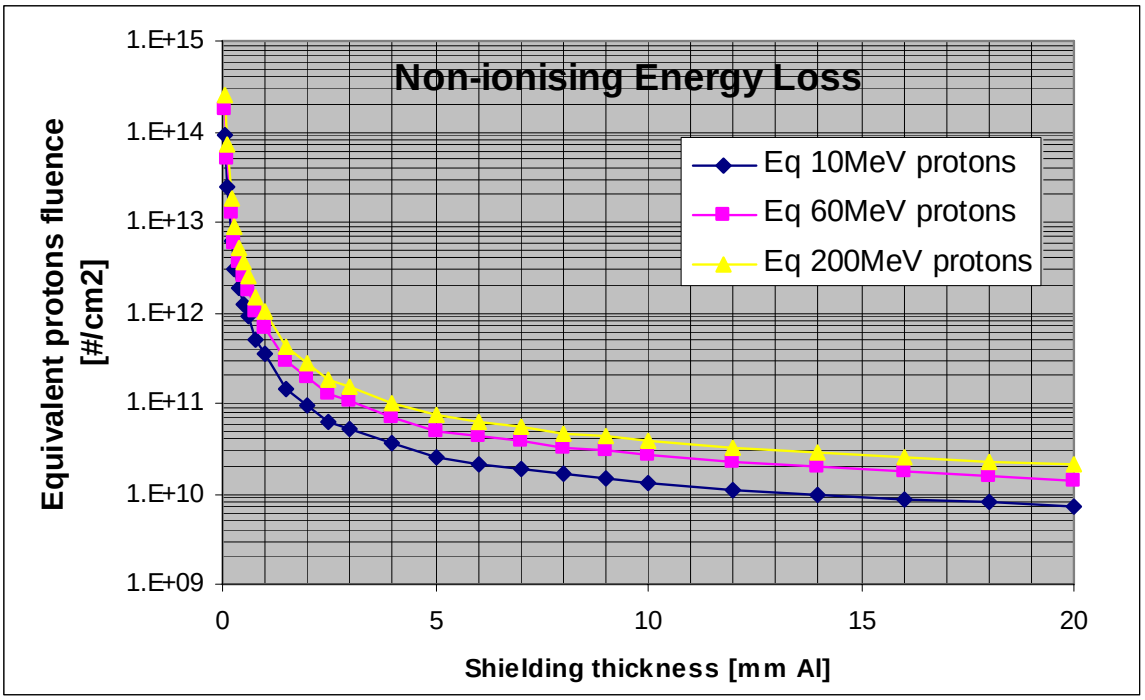

Figure 12: Non-ionising energy loss as a function of Al shielding for the Proba3 orbit in terms of equivalent 10Mev, 60MeV and 200MeV proton fluence

Shielding Thickness [mm]	Non-ionising energy loss [MeV/g(Si)]	Equivalent proton Fluence [#/cm2]		
		10MeV	60MeV	200MeV
0.05	6.15E+11	8.91E+13	1.78E+14	2.56E+14
0.1	1.72E+11	2.49E+13	4.96E+13	7.15E+13
0.2	4.30E+10	6.24E+12	1.24E+13	1.79E+13
0.3	2.07E+10	3.01E+12	6.00E+12	8.65E+12
0.4	1.26E+10	1.82E+12	3.64E+12	5.24E+12
0.5	8.73E+09	1.27E+12	2.53E+12	3.64E+12
0.6	6.23E+09	9.04E+11	1.80E+12	2.60E+12
0.8	3.55E+09	5.15E+11	1.03E+12	1.48E+12
1	2.41E+09	3.50E+11	6.98E+11	1.01E+12
1.5	1.02E+09	1.47E+11	2.94E+11	4.23E+11
2	6.66E+08	9.65E+10	1.93E+11	2.78E+11
2.5	4.31E+08	6.25E+10	1.25E+11	1.80E+11
3	3.58E+08	5.19E+10	1.04E+11	1.49E+11
4	2.47E+08	3.58E+10	7.15E+10	1.03E+11
5	1.73E+08	2.51E+10	5.01E+10	7.21E+10
6	1.50E+08	2.17E+10	4.34E+10	6.25E+10
7	1.31E+08	1.89E+10	3.78E+10	5.44E+10
8	1.13E+08	1.64E+10	3.27E+10	4.71E+10
9	1.03E+08	1.49E+10	2.97E+10	4.27E+10
10	9.27E+07	1.34E+10	2.68E+10	3.86E+10
12	7.59E+07	1.10E+10	2.20E+10	3.16E+10
14	6.75E+07	9.78E+09	1.95E+10	2.81E+10
16	5.96E+07	8.64E+09	1.72E+10	2.48E+10
18	5.47E+07	7.93E+09	1.58E+10	2.28E+10
20	4.96E+07	7.18E+09	1.43E+10	2.06E+10

Figure 13: Non-ionising energy loss as a function of Al shielding for the Proba3 orbit

4.8 References

[1] Hess W.N., "The Radiation Belt and Magnetosphere", Blaisdell Publ. Co.,1968

[2] Daly, E.J., "The Radiation Belts", Radiation Physics and Chemistry 43, 1, pp.1-18 (in Special Issue on Space Radiation Environment and Effects), 1994

[3] ECSS-E-10-12, Space engineering – Methods for the calculation of radiation received and its effects and a policy for design margins

[4] Vette J.I. "The AE-8 Trapped Electron Model Environment", NSSDC/WDC-A-R&S Report 91-24, NASA-GSFC (1991)

[5] Sawyer D.M. and Vette J.I., "AP8 Trapped Proton Environment For Solar Maximum and Solar Minimum", NSSDC WDC-A-R&S 76-06, NASA-GSFC (1976).

[6] A Sicard-Piet, S. A.Bourdarie, D. M. Boscher, R. H. W. Friedel, M. Thomsen, T. Goka, H.Matsumoto, H. Koshiishi, "A new international geostationary electron model: IGE-2006, from 1 keV to 5.2 MeV", Space Weather, 6, S07003, doi:10.1029/2007SW000368, 2008.

[7] Xapsos, M. A., G.P. Summers, J.L. Barth, E. G. Stassinopoulos and E.A. Burke, "Probability Model for Cumulative Solar Proton Event Fluences", IEEE Trans. Nucl. Sci., vol. 47, no. 3, June 2000, pp 486-490

[8] Feynman, J., T. P. Armstrong, L. Dao-Gibner, and S. Silverman, New Interplanetary Proton Fluence Model, *J. Spacecraft and Rockets, 27*, 403, 1990.

[9] King, J.H., "Solar Proton Fluences for 1977-1983 Space Missions", J. Spacecraft & Rockets 11, 401, (1974)

[10] Mathews J. and Towheed S., OMNIWeb, http://nssdc.gsfc.nasa.gov/omniweb/ mathews@nssdc.gsfc.nasa.gov, Code 633, NASA GSFC, Greenbelt, MD 20771, USA

[11] National Geophysical Data Center, "Space Environment Data from NOAA's GOES Satellites", National Geophysical Data Center, Code E/GC2, Dept. 946 325 Broadway Boulder Co 80303 3328 USA., also Space Physics Interactive Data Resource at http://www.ngdc.noaa.gov:8080/

[12] A.J. Tylka et al. "CREME96: A Revision of the Cosmic Ray Effects on Micro-Electronics Code", IEEE Trans. Nucl. Sci. NS-44, 2150-2160 (1997).

[13] Adams J.H., Silberberg R. and Tsao C.H., "Cosmic Ray Effects on Microelectronics, Part I: The Near-Earth Particle Environment", NRL Memorandum Report 4506, Naval Research Laboratory, Washington DC 20375-5000, USA (1981).

[14] R.A. Nymmik, M.I. Panasyuk, T. I. Pervaja, and A.A. Suslov "A Model of Galactic Cosmic Ray Fluxes", by, Nucl. Tracks & Radiat. Meas, 20, 427-429 (1992)

[15] Seltzer S., 'SHIELDOSE: A Computer Code For Space Shielding Radiation Dose Calulations', NBS Technical Note 1116, National Bureau of Standards, May 1980 .

[16] Petersen E.L., "Approaches to Proton Single-Event-Rate Calculation", IEEE Trans. Nucl. Sci. NS-43, 2 (special issue on Single Event Effects and the Space Environment), 496 (1996)

[17] Pickel J.C., " Single-Event Effects Rate Prediction", IEEE Trans. Nucl. Sci. NS-43, 2 (special issue on Single Event Effects and the Space Environment), 483 (1996).

[18] Tada H.Y., Carter J.R, Anspaugh B.E. & Downing R.G, " Solar Cell Radiation Handbook", 3rd Edition, JPL Publn. 82-69 (1982); Anspaugh B.E, "GaAs Solar Cell Radiation Handbook", JPL Publn. 96-9 (1996).

[19] Marvin, D. C., Assessment of Multijunction Solar Cell Performance in Radiation Environments, Aerospace Report No. TOR-2000(1210)-1, 2000.

[20] Rodgers D.J, Hunter K.A and Wrenn G.L, The Flumic Electron Environment Model, Proceedings 8th Spacecraft Charging Technology Conference, Huntsville Alabama, 2003

[21] D.J. Rodgers, K.A. Ryden, P.M. Latham, L. Levy and G. Panabiere, "Engineering Tools for Internal Charging", ESA Contract Final Report DERA/CIS(CIS2)/7/3/36/2/4/FINAL, January 1999. http://www.estec.esa.nl/wmwww/WMA/reports/idc/final_report.pdf

[22] "Avoiding problems caused by spacecraft on-orbit internal charging effects", NASA Technical handbook, NASA-HDBK-4002, February 1999, can be obtained via http://standards.nasa.gov

[23] Hopkinson G.R., Dale C.J. and Marshall P.W., "Proton Effects in Charge-Coupled Devices", IEEE Trans. Nucl. Sci. NS-43, 2 (special issue on Single Event Effects and the Space Environment), 614 (1996).

[24] ECSS-E-20-06, Space Engineering, Spacecraft Charging

5 PARTICULATES

5.1 Introduction

Every spacecraft in Earth orbit is exposed to a certain flux of micrometeoroids and man made space debris. Collisions with these particles will take place with hypervelocity speed.

Meteoroids are particles of natural origin. Nearly all meteoroids originate from asteroids or comets. The natural meteoroid flux represents, at any instant, a total of about 200 kg of mass within 2000 km of the Earth's surface [1]. Meteoroids that retain the orbit of their parent body can create periods of high flux and are called streams. Random fluxes with no apparent pattern are called sporadic.

Space debris is man-made. Since 1957, more than 3500 launches have led to a population (1998) of approximately 9000 trackable objects (i.e. larger than about 10 cm in Low Earth Orbits (LEO)) in space. More than 90% of these objects are space debris, i.e., man-made objects that do not serve any useful purpose. The number of space debris objects larger than 1 cm is estimated to be of the order of 500000 to 700000 (2007). Smaller particles are far more abundant still. Space debris is mainly concentrated in LEO (below 2000km) and in GEO. Spacecraft in the Proba3 orbit will mainly encounter fluxes from debris in high inclination orbits.

The damage caused by collisions with meteoroids and space debris will depend on the size, density, speed and direction of the impacting particle and on the shielding of the spacecraft. Submillimeter sized particles can cause pitting and cratering of outer surfaces and lead to degradation of optical, electrical, thermal, sealing or other properties. Larger particles can puncture outer surfaces and may cause damage to structure or equipment by penetration and spallation.

Flux models have been developed for both micrometeoroids and space debris. The resulting damage can be assessed through empirically derived design equations which give penetration capabilities, crater sizes, etc. as function of the particle parameters and target properties.

5.2 Analysis techniques

For meteoroids and the abundant smaller space debris particles, which cannot be tracked, statistical flux models have to be used. The meteoroid and debris fluxes are usually specified as a time-averaged flux, F_r, against a single sided, randomly tumbling surface. Flux is defined as number of intercepted objects per unit time and area. The relevant area for F_r is the actual outer surface area of a spacecraft element.

For spacecraft, which fly with a fixed orientation, the directionality of the meteoroid and orbital debris fluxes must be taken into account. Most impacts from both, meteoroids and space debris

will occur on forward facing (+X) surfaces. The number of impacts, N, increases linearly with exposed area and with exposure time:

$$N = F \times A \times T$$

where F is the number of impacts per unit area, A is the total exposed area and T is the exposure time.

The numbers of impacts from meteoroids and space debris can be summed to obtain the total number of impacts:

$$N_{tot} = N_{met} + N_{deb}$$

Once N has been determined, the probability of exactly n impacts occurring in the corresponding time interval is given by Poisson statistics:

$$P_n = (N^n)/n!) \; . \; e^{-N}$$

The probability for no impacts, P_0 is thus given by:

$$P_0 = e^{-N}$$

For values of $N << 1$ the probability, Q, for at least one impact ($Q = 1 - P_0$) is equal to N:

$$Q = 1 - e^{-N} \approx 1 - (1 - N) = N$$

5.3 Model presentation

5.3.1 METEOROIDS

For meteoroids, the isotropic flux model given in [2] shall be used. This model gives the total average meteoroid **flux** (sporadic + stream average) in terms of the integral flux $F_{met,0}$ which is the number of particles with mass m or larger per m^2 per year impacting a randomly-oriented flat plate under a viewing angle of 2π . The unshielded interplanetary flux at 1 AU distance from the sun is according to the model described by the analytical formula:

$$F_{met,0}(m) = 3.15576 \times 10^7 (F_1(m) + F_2(m) + F_3(m))$$

where:

$$F_1(m) = (2.2 \times 10^3 \; m^{0.306} + 15)^{-4.38}$$

$$F_2(m) = 1.3 \times 10^{-9} (m + 10^{11} \; m^2 + 10^{27} \; m^4)^{-0.36}$$

$$F_3(m) = 1.3 \times 10^{-16} (m + 10^6 \; m^2)^{-0.85}$$

with m in grams.

Meteoroid **velocities** near Earth can range from 11 to 72 km/s. The velocity distribution with respect to Earth to be used with the isotropic reference flux model given in [2] is (number per km/s):

$$g(v) = \begin{cases} 0.112 & \text{if } 11.1 \le v < 16.3 \text{ km/s} \\ 3.328\times10^{5}\, v^{-5.34} & \text{if } 16.3 \le v < 55.0 \text{ km/s} \\ 1.695\times10^{-4} & \text{if } 55.0 \le v < 72.2 \text{ km/s} \end{cases}$$

The average velocity of this distribution is close to 17 km/s.

The unshielded flux $F_{met,0}$ has to be modified to account for the **gravitational attraction** (which enhances the meteoroid flux in the Earth proximity) and the geometrical shielding of the Earth (which reduces the flux). The gravitational enhancement factor G_e is according to [1]:

$$G_e = 1 + R_E / r$$

where

R_E is the mean Earth radius
r is the orbit radius

The **Earth shielding** factor, s_f, for a given surface depends on the altitude and on the relative orientation of the surface normal with respect to the Earth direction. For the Proba3 orbit the following values are obtained (according to [3]):

$$s_f = \begin{cases} 0.95 & \text{for a surface pointing in the +Z direction (towards Earth)} \\ 1 & \text{for a surface pointing in the -Z direction} \\ 0.988 & \text{For a random oriented surface} \end{cases}$$

The meteoroid flux to an Earth orbiting spacecraft is then given by:

$$F_{met} = F_{met,0} \times G_e \times s_f$$

The **mass density** of meteoroids varies widely from about 0.15 g/cm^3 to 8 g/cm^3.

For the **directional distribution** the annual averaged meteoroid flux is usually considered to be omnidirectional with respect to the Earth surface. Relative to a spacecraft with fixed orientation w.r.t. the flight direction the meteoroid flux has a directional dependence, introduced by the motion of the spacecraft together with the Earth shielding effect. The directional dependence of meteoroids has then to be calculated numerically by converting the omnidirectional flux to the flux on a specific surface with given surface orientation and spacecraft velocity vector.

The meteoroid flux model described above gives a yearly average. **Meteoroid streams** are accumulations of meteoroids with nearly identical heliocentric orbits. Relative to Earth all particles of a given meteoroid stream have nearly identical impact directions and velocities. Encounters with meteoroid streams typically lasts from a few hours to several days.

At peak activity stream fluxes can exceed the sporadic background fluxes by a factor 5 or more. Occasionally, very high fluxes (meteoroid storms, the visible meteor background flux can be exceeded by a factor 10000 or more) can be encountered for short periods (1-2 hours).

Meteoroid streams are believed to consist of relative large particles only (mass > 10^{-8} - 10^{-6} g) with low density (0.5-1.0 g/cm^3).

Tailoring guidelines

Values for average mass densities of meteoroids are:

Low:	1.0 g/cm^3
Nominal:	2.5 g/cm^3
High:	4.0 g/cm^3

For analysis of effects the nominal value of 2.5 g/cm^3 shall be used.

For the assessment of impact effects the full velocity distribution and the full directional impact distribution of meteoroids should be used.

For a preliminary analysis a constant meteoroid impact velocity of 20 km/s and an impact angle of 45º (from the surface normal) shall be used.

A spherical shape shall be assumed to convert particle masses and diameters.

For Proba3 the yearly averaged model can be used.

5.3.2 SPACE DEBRIS

For space debris the ESA MASTER-2005 model [5] shall be used. The MASTER-2005, uses a semi-deterministic approach which represents the debris environment by modelling its history from the beginning of spaceflight to present. It uses separate source terms for the debris population: launches, explosions and collisions and follows their orbital evolutions. The model includes additional non-fragmentation source distributions like paint flakes, Aluminium Oxide particles from solid rocket motor burns and Sodium/Potassium droplets. These non-fragmentation sources mainly contribute to the small size population. The model is also derived from recent radar measurements and impact data from retrieved surfaces. Collision probability equations are used to relate the orbital element distributions of the population to the flux measured on a spacecraft, and it provides directional information of the impacting flux. The model is applicable for particle sizes larger than 1 micron. Impact **velocities** at the Proba3 altitude can range from 0 to about 8 km/s with an average velocity of 4 km/s. The average **density** of smaller space debris particles is thought to be in the range 2.8 - 4.7 g/cm^3.

Tailoring guidelines

Nominal and worst case debris model parameters and mass densities are:

Parameter	Nominal	Worst case
ref. Mission year, t	Middle	Last
Debris density ρ [g/cm^3]	4.0	8.0

For design purposes the nominal parameter values shall be used. A spherical shape shall be assumed to convert particle masses and diameters. The default growth rates for the respective models shall be used. For the assessment of impact effects the full velocity and directional distribution of space debris should be used. For a preliminary analysis a constant debris impact velocity of 4 km/s and an impact angle of 45º shall be used.

5.4 Reference data

5.4.1 STATISTICAL FLUX MODELS

Cumulative meteoroid and space debris fluxes (i.e. fluxes of particles of given size or larger) can be obtained directly from the flux models. Figure 1 gives the number of impacts /m^2/year from one side to a randomly oriented plate for a range of minimum particle sizes. The results are for the Proba3 orbit . The meteoroid fluxes are from the model given in 5.3.1. For meteoroids a density of ρ = 2.5 g/cm^3 and the assumption of spherical shape were used to convert masses to diameters. The MASTER-2005 model [5] was used for the debris fluxes. Figure 2 gives the same data in tabulated form.

Meteoroids directionality

The present meteoroid flux model assumes an isotropic flux w.r.t. the Earth surface. For an orbiting spacecraft the Earth shielding and the spacecraft motion both introduce a directional dependence. The Earth shielding factor is given in 5.3.1. The directionality caused by the spacecraft motion leads to increased fluxes on forward facing surfaces and to reduced fluxes on trailing surfaces. Combining the two factors the following flux ratios for meteoroids are found for the Proba3 orbit (using the velocity distribution from 5.3.1):

front/random	≈1.5
front/rear	≈ 2.5
space face/Earth face	≈1.05

As resulting effects like penetration depth or impact plasma generation also depend on parameters like impact velocity and angle, the directional ratios for these effects can be considerably different from those given above.

Debris directionality

The debris fluxes will be different for the various surface orientations. The highest space debris fluxes are encountered by forward (ram) facing surfaces. The flux ratio oriented/random surface depends on the particle size and the orbit. Typical ratios for the Proba3 orbit for 1mm debris particles are (using the models described in 5.3.2):

front/random	≈2.2
front/rear	≈ 290

5.5 Model uncertainties

The meteoroid and space debris environment flux models given above contain several known approximations and other uncertainties.

5.5.1 METEOROIDS

According to [1] uncertainties in the meteoroid models mainly result from uncertainties in particle densities and masses. Fluxes for meteoroids larger than 10^{-6} g are well defined, but the associated masses are quite uncertain. The mass density of meteoroids spans a wide range, from about 0.15 g/cm^3 to values as large as 8 g/cm^3. At a set mass this implies an uncertainty in the flux of a factor 0.1 to 10. For meteoroids smaller than 10^{-6} g flux uncertainties at a given mass are estimated to be a factor of 0.33 to 3.

5.5.2 SPACE DEBRIS

The space debris flux models were developed as a best estimate rather than a conservative one. In [1] uncertainties for debris fluxes in different size regimes are quoted. These factors give the 90 % confidence level that the real debris flux is within a bandwidth defined by the model flux multiplied by the uncertainty factors. Uncertainty factors for the Proba3 orbit will be higher than those quoted in [1]. Estimated uncertainty factors are:

Particle size	**Uncertainty factor**
d > 10 cm	0.5 to 2
0.05 cm < d < 10 cm	0.2 to 5

0.001 cm < d < 0.05 cm	0.1 to 10
d < 0.001 cm	0.02 to 50

The given uncertainty factors for debris fluxes < 0.05 cm reflect the fact that these fluxes are based on simulations and simple extrapolations only. No measurements are available for these sizes and the true debris population is essentially unknown. Other uncertainties of the debris model include the debris density and shape, the annual growth rates, the velocity distribution (especially for low impact velocities) and the dependence on solar activity.

5.6 Damage assessment

In this section a brief general overview of damage assessment criteria and procedures is given. For each individual project the damage assessment has to be tailored according to the specific conditions and requirements (e.g. shielding, damage criteria, required reliability, etc.). Any damage assessment depends to a large extent on the relevant failure criteria. Possible failure criteria include:

- cratering (sensor degradation, window blinding, surface erosion)
- larger craters (sealing problems, short circuits on solar arrays)
- impact generated plasma (interference, discharge triggering)
- wall penetration (damage, injury, loss of liquid or air)
- burst, rupture (pressurised parts)
- structural damage

For a quantitative damage and risk assessment, so-called damage or design equations for the given shielding configuration are needed. They give shielding thresholds or hole sizes for given impacting particle parameters and failure mode. One of the most widely used damage equation gives the threshold thickness for penetration of single metal plates (thin plate formula):

$$t = k_m \, m^{0.352} \, \rho^{0.167} v^{0.875}$$

where:

t: threshold thickness for penetration [cm]

k_m: material constant, 0.55 for Aluminium

m: mass of projectile [g]

ρ: density of projectile [g/cm^3]

v: normal impact velocity component of projectile [km/s]

A puncture occurs whenever the threshold thickness for an impacting particle with given mass, density and velocity exceeds the shielding thickness of the surface under consideration. Finding a realistic damage equation for a given shielding configuration can be problematic. The translation of a failure mode to a damage equation can be difficult. Many damage equations for different types of shields and for different velocity regimes have been developed. However, for most materials, compounds, and shielding concepts no specific damage equation is available.

Sometimes scaled effective thickness in combination with known damage equations can be used for a first assessment. For impact damage and risk assessments secondary ejecta should be considered as well. Every hypervelocity impact leads to the ejection of secondary particles which can impact other surfaces (depending on the spacecraft geometry). The total mass of the ejected particles can exceed the mass of the primary impactor by orders of magnitude. Secondary particles will be typically ejected within a cone around the impact direction. Their velocities are typically below 2 km/s. At present, quantitative models of secondary ejecta are not mature enough to be used as standard.

5.7 Analysis tools

Several numerical tools have been developed to perform impact and impact risk analyses. One possible tool is the ESABASE/DEBRIS [6]. It is a statistical tool and was developed for a detailed impact risk assessment of smaller, non-trackable particles. ESABASE/DEBRIS is a fully three dimensional numerical analysis tool including directional and geometrical effects and spacecraft shielding considerations. It is based on environment and particle/wall interaction models and includes the reference meteoroid and space debris flux models defined in this document. The user specifies the mission, spacecraft geometry, attitude and shielding as well as the particle type, size and velocity range to be analysed. The computed output includes:

- the number of impacts,
- the resulting number of damaging impacts taking into account the spacecraft shielding and damage assessment equations,
- the mean particle impact velocity (amplitude and direction),
- the numbers of craters of specified size,
- the probability of no failure.

5.8 Figures

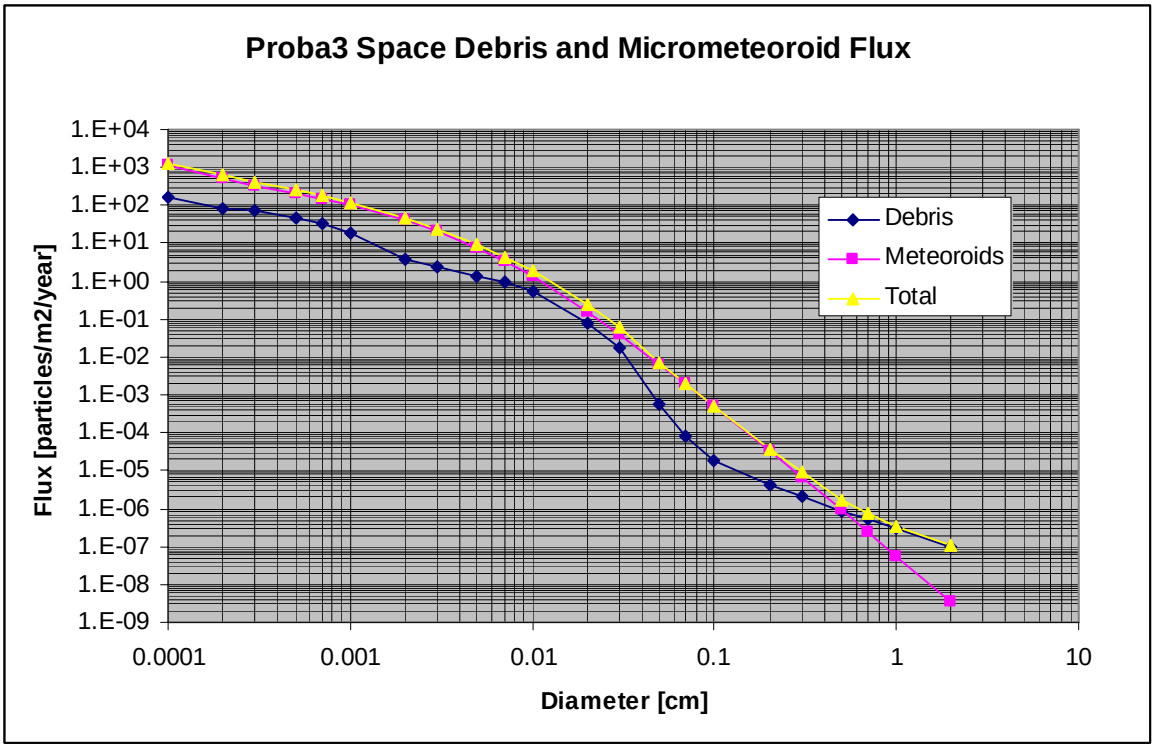

Figure 1: Cumulative number of impacts, N, to a randomly oriented plate for a range of minimum particle sizes. The results are for an orbit with semi-major axis = 42378 km, eccentricity= 0.830617, I = 17.8 deg, R.A. of ascending node = 68 deg, argument of perigee = 180 deg. The debris fluxes were obtained by the MASTER 2005 model for an epoch of May 1st, 2005. The meteoroid fluxes were obtained by the model from Gruen et al.

Figure 2: Cumulative number of impacts, N, to a randomly oriented plate for a range of minimum particle sizes. The results are for an orbit with semi-major axis = 42378 km, eccentricity= 0.830617, I = 17.8 deg, R.A. of ascending node = 68 deg, argument of perigee = 180 deg. The debris fluxes were obtained by the MASTER 2005 model for an epoch of May 1st, 2005. The meteoroid fluxes were obtained by the model from Gruen et al.

Diameter [cm]	**N_{deb}** [#/m2]/year]	**N_{met}** [#/m2]/year]	**N_{tot}** [#/m2]/year]
0.0001	1.64E+2	1.15E+3	1.31E+3
0.0002	8.64E+1	5.37E+2	6.23E+2
0.0003	7.60E+1	3.39E+2	4.15E+2
0.0005	4.87E+1	1.99E+2	2.48E+2
0.0007	3.27E+1	1.44E+2	1.77E+2
0.001	1.83E+1	1.01E+2	1.19E+2
0.002	3.73E+0	4.24E+1	4.61E+1
0.003	2.30E+0	2.17E+1	2.40E+1
0.005	1.37E+0	7.77E+0	9.14E+0
0.007	9.78E-1	3.49E+0	4.47E+0
0.01	5.37E-1	1.35E+0	1.89E+0
0.02	7.57E-2	1.62E-1	2.38E-1
0.03	1.75E-2	4.10E-2	5.85E-2
0.05	5.99E-4	6.61E-3	7.21E-3
0.07	7.79E-5	1.90E-3	1.98E-3
0.1	1.84E-5	4.92E-4	5.10E-4
0.2	4.36E-6	3.36E-5	3.80E-5
0.3	2.10E-6	6.82E-6	8.92E-6
0.5	8.06E-7	9.02E-7	1.71E-6
0.7	5.46E-7	2.36E-7	7.82E-7
1.0	2.87E-7	5.69E-8	3.44E-7
2.0	1.00E-7	3.54E-9	1.04E-7

5.9 References

[1] Anderson B.J., "Natural Orbital Environment Guidelines for Use in Aerospace Vehicle Development", by:, editor and R.E. Smith, compiler; NASA TM 4527, chapter 7, June 1994

[2] Grün E., H.A. Zook, H. Fechtig and R.H. Giese, "Collisional Balance of the Meteoritic Complex", Icarus, Vol. 62, p.244, 1985

[3] ECSS-E-ST-10-04C, Space Engineering, Space Environment

[4] Jenniskens P., "Meteor Stream Activity"; Astron. Astrophys. Vol. 287, pp 990-1013, 1994

[5] MASTER 2005 DVD, ESA-SD-DVD-01, Release 1.0, April 2006

[6] G.Drolshagen and J.Borde, 'ESABASE/DEBRIS, Meteoroid/Debris Impact Analysis, Technical Description', ref. ESABASE--GD--01/1, 1992

6 CONTAMINATION

6.1 Introduction

This chapter deals with the induced molecular and particulate (solid or liquid) environment in the vicinity of and created by the presence of the Proba3 spacecraft in its orbit. It is meant mainly to aid in the definition of the contamination environment (foreign or unwanted matter that can affect or degrade the performance of any component when being in line of sight with that component or when residing onto that component). The relevant computer models and tools are also presented.

The quantitative modelling of the contamination environment is very complex. This is due to the high number of materials involved, with a variability of outgassing characteristics. Furthermore, there are interactions of the outgassing products with surfaces, residual gas and with other environmental parameters such as solar radiation, atomic oxygen.

The contamination analysis, which necessarily is very much dependent of a specific application, cannot be more detailed in this specification. ECSS-Q-70-01 [1] defines amongst others the requirements to be followed and guidelines to be taken into account in order to control the particulate and molecular contamination within the specified limits during a mission.

It is the responsibility of the user:

- to estimate the sensitivity of his system/equipment with regard to contamination
- to identify the contamination sources on his experiment
- to evaluate with all appropriate means the expected contamination levels/quantities present in critical areas, taking into account the mechanisms of transport and fixation of contaminants.

6.2 Molecular contamination

6.2.1 SOURCES OF MOLECULAR CONTAMINATION

Outgassing of Organic Materials

Outgassing of organic materials can be approached as a surface evaporation combined with a diffusion for bulk contaminant species. These species can be either initially present components, or decomposition products.

Initially present outgassing species can be: water, solvents, additives, uncured monomeric material, lubricants, ground contamination species, due to e.g. processes, test, storage, handling, pre-launch and launch.

The decomposition products are due to exposure of molecular materials to other environments, such as: thermal, solar radiation, electromagnetic and charged particles, atomic oxygen , impacts by micrometeoroids or debris, electrical discharges and arcing

These products consist of lower molecular weight (higher volatility) species than the original species.

Plumes

Plume species can result from combustion, unburned propellant vapours, incomplete combustion products, sputtered material and other degradation products from a propulsion or attitude control system and its surroundings swept along with the jet.

Plumes can also be produced by dumps of gaseous and liquid waste materials of the environment control and life support systems in manned spacecraft or by leaks in systems or internal payloads.

Contamination of surfaces not in direct view is possible due to ambient scattering (collisions with other residual atmosphere species), self scattering (collisions with other identical or different contaminant species) or ionisation of the molecules under radiation, e.g. UV or particles, and subsequent attraction to a charged surface

Pyrotechnics and release mechanisms

During operation of pyrotechnics or other release mechanisms gases can evolve.

Secondary sources

A surface can act as a secondary source if an incoming contaminant molecule will reflect (not accommodate stick or condense on the surface) or if it has a limited residence time on that surface. Secondary sources can for example be solar panels having a higher temperature than the surrounding surfaces.

6.2.2 TRANSPORT MECHANISMS

Apart from the direct flux there are different transport mechanisms by which a contaminant molecule can reach a surface. Surface accommodation occurs when a molecule becomes attached to a surface long enough to come into a thermal equilibrium with that surface (an accommodation coefficient can be defined as a measure for the amount of energy transfer between the contaminant molecule and the surface). It is useful to define the concept of a sticking coefficient as the probability that a molecule, colliding with a surface, will stay onto that surface for a time long compared to the phenomena under investigation. The sticking coefficient is a function of such parameters as contamination/surface material pairing, temperature, photo-polymerisation, reactive interaction with atomic oxygen.

Reflection on surface

A molecule will reflect on a surface when the accommodation coefficient during a collision is zero, i.e. when there is no energy transfer between the molecule and the surface during that collision. A reflection of a molecule is always specular, although this will be dependent on surface roughness, RMS)

Re-evaporation from surface

A molecule having a non-zero residence time can re-evaporate from a surface. Re-evaporation is diffuse, i.e. the molecule is leaving the surface following a Lambertian distribution law.

Migration on surface

A molecule accommodated on a surface can migrate over that surface.

Collision with residual (natural) atmosphere

The contamination environment shall take into account the collision between the contamination species and the residual atmosphere. This interaction results in an ambient scattering of the contamination species, and can sometimes lead to an increase in the local pressure.

Collision with other outgassed molecules

The contamination environment shall take into account the collision between two contamination molecules. This interaction results in self-scattering of the contamination species.

Ionisation by other environmental parameters

A molecule can be ionised due to interaction with (V)UV or charged particles (electrons, protons, ions) and subsequently be attracted by a charged surface

Permanent Molecular Deposition (PMD)

Molecular matter can permanently stick onto a surface (non-volatile under the given circumstances) as a result of reaction with surface material, UV-irradiation or residual atmosphere induced reactions (e.g. polymerisation, formation of inorganic oxides).

6.3 Particulate contamination

6.3.1 SOURCES OF PARTICULATE CONTAMINATION

Sources inherent to materials: particles originating from manufacturing (machining, sawing), handling (e.g. for brittle materials such as certain paints) or wear (friction); degradation of binder under different environments (e.g. AO, UV...) resulting in loose filler; crack formation and subsequent flaking as a result of thermal cycling; formation of particles due to oxidation in an Atomic Oxygen environment.

Sources external to materials: dust particles can be caused by atmospheric fall-out (dust) during assembly, integration and storage or by human sources during such activities (hair, skin flakes, lints or fibres from garments...); particles can be produced during spacecraft propulsion or attitude control operations, the functioning of moving parts (such as shutters), and water dumps; particles can result from micrometeoroid or debris impacts on materials.

6.3.2 TRANSPORT MECHANISMS

Particles can be transported by vibrations due to launch, (attitude control) manoeuvring and docking. Pyrotechnic shocks can cause particles to migrate from one surface to another.

Particles can be charged due to their interaction with ambient plasma or photo emission, and subsequently attracted by electrically charged surfaces.

For specific missions other mechanisms can have an effect on the particles, such as: drag, due to the residual atmosphere in the lowest Earth orbits; radiation pressure due to solar radiation; gravitational tide, e.g. re-attraction to spacecraft.

6.4 Effect of contamination

The primary concerns of contamination are related to the degradation of spacecraft elements or sub-system performances due to the presence of :

- deposited species onto a critical surface:

  (thermo-)optical properties, such as transmission, reflection, absorption, scattering, tribological properties, outgassing of lubricant, friction due to particles electrical properties, such as surface conductivity, secondary emission and photo-emission.

- glow or other surface/gas reactions
- free flying species in the field of view of sensors:

  light scattering (star trackers)
  light absorption
  background increase (natural environment analysis)

The effect of a contamination can be altered by the exposure to other environmental parameters, e.g. UV can increase the absorption due to photo-degradation (darkening) of the deposited contaminant, Atomic Oxygen can have a cleaning-up effect on hydrocarbon material, but can also form non-volatile SiOx that can further trap other contaminants.

6.5 Models

Worst case outgassing modelling can be based on screening thermal vacuum test (VCM-test) to determine the outgassing properties of materials. The test is described in ECSS-Q-70-02 and ASTM-E595-90 [2] [3]. The test results are:

TML -- Total Mass Loss (sum of condensable and non-condensable material), measured ex-situ as a difference of mass before and after exposure to a vacuum under the conditions specified in the outgassing test.

RML -- Recovered Mass Loss (difference between the initial mass and the mass after re-climatisation after the vacuum test, showing the amount on non-water products in the total mass loss).

CVCM -- Collected Volatile Condensable Material (Low Vapour Pressure, condensable material), measured ex-situ on a collector plate after exposure (to a vacuum) under the conditions specified in the outgassing test.

TML, RML and CVCM are normally expressed in % of the initial mass of the material.

More sophisticated outgassing/condensation models will take into account the data of outgassing or mass flow rates, surface accommodation and sticking coefficients as obtained by e.g. the VBQC-test [4] or the ASTM E-1559 test [5].

6.5.1 OUTGASSING SOURCES

For a material that outgassses at a constant rate, independently of the quantity present, such as e.g. during evaporation or sublimation from a bulk, the process can be described as a zero order reaction.

$$dm/dt = k$$

with:

dm/dt	outgassing rate in $g \cdot cm^{-2} \cdot s^{-1}$
k	reaction constant

The weight-loss through evaporation, at a temperature T is given by [6]

$$dm/dt = 0.04375 \cdot P_s \cdot (M/T)^{1/2}$$

with:

P_s	Vapour Pressure in mbar
dm/dt	weight-loss per unit area in $g \cdot cm^{-2} \cdot s^{-1}$
M	Molecular mass
T	Temperature in K

The outgassing is often described as a first order reaction [7], i.e. the material outgasses at a rate that is proportional to the mass available, and using Arrhenius law for the temperature dependency. Important parameters for the outgassing rate are temperature, exposed surface area (or the surface available for evaporation), surface morphology, dimensions of the material (characteristic dimension, thickness).

$$dm/dt = - m/\tau$$

with τ being a temperature dependent time constant of the outgassing phenomenon. Integration gives:

$$m = m_0 \cdot \exp(-t/\tau)$$

Assuming the Arrhenius relation to be valid

$$\tau = \tau_0 \exp(-E/RT)$$

it is possible to determine the outgassing as function of temperature.

The mass loss can be expressed as

$$m_{loss} = m_o \cdot m = m_o \cdot (1 - \exp(-t/\tau)$$

Plumes

Evaluation of plumes of thrusters or vents is often described by specific application related models. Parametric descriptions of plumes constitute an interesting alternative to spacecraft designers.

The mass flux Φ of a plume can be expressed in the most generic form

$$\Phi (r, \Theta) = f(r, \Theta, dm/dt)$$

with

- $\Phi(r, \Theta)$ flux at a given position from the vent
- r radial distance from the vent
- Θ angle from the centerline of the vent
- dm/dt Mass flow from the vent

where moreover the function *f* will depend on the plume type. However this formula can in general be reduced in a good approximation to the product

$$\Phi (r, \Theta) = A \cdot (dm/dt) \cdot f_1(\Theta) \cdot r^{-2}$$

where A is a normalisation coefficient.

For a thruster, the function f_1 is peaked around Θ=0 and can be expressed as a sum of decreasing exponentials [8] or as a (high) power law of cos(Θ) or both [9]. It is in some extent specific of each thruster.

Plumes from vents are more standard and the f_1 function can consequently be fixed : the mass flux is approximated by the following engineering model

$$\Phi (r, \Theta)=((n+1)/(2 \pi)) \cdot (dm/dt) \cdot \cos^n(\Theta) \cdot r^{-2}$$

where $1 \leq n \leq 2$ are typical values used for design. The divergence is larger than the one of thrusters.

6.5.2 TRANSPORT OF MOLECULAR CONTAMINANTS

Transport between surfaces

This section only deals with the methods and models for transport of neutral molecules. There is no available model of ion transport devoted to contamination.

Three levels of complexity and accuracy in modelling the transport of neutral molecular contaminants can be distinguished.

Simplest view factors

This model simulates collisionless transport. In such a case the fraction of contaminants coming from surface j to surface i is given by the view factor V_{ij} of surface i seen from surface j (including the cosine factor coming from lambertian emission law). These view factors are similar to the ones of radiative thermal analysis. They can be computed geometrically or by Monte-Carlo ray tracing. The incident mass on a surface i is then given by

$$S_j \, V_{ij} \cdot dm_j/dt$$

where j runs over all surfaces and dm_j/dt denotes the outgassing mass rate of surface j.

Simplified Monte-Carlo

Collisions of contaminants are simulated in a simplified way, the density and speed of possible partners for molecular collisions are given a priori:

- for ambient scatter, the ambient density and speed are easily known, but wakes (or 'shades') are usually not treated,
- for self-scatter, the contaminant density is very simplified and usually taken proportional to $1/r^2$ and with spherical symmetry.

This method is usually limited to one collision per molecule because the uncertainties due to the densities given a priori increase with collision number. This effective view factors can conveniently be computed by Monte-Carlo ray-tracing method.

Both methods can include other contaminant sources such as vents and plumes. The view factors are then replaced by interception factors.

True Monte-Carlo (Direct Simulation Monte-Carlo DSMC)

This computes multiple collisions in a realistic way. The collision probabilities are computed auto-coherently from the densities given by the simulation. This method is far more time consuming and requires more work for programming (in particular it requires a meshing of volume and not only of spacecraft surfaces).

Either method can be better suited, depending on the spacecraft configuration. A potential contamination of a sensitive protected surface through multiple collisions shall require a precise DSMC simulation. In simpler cases, when contamination essentially happens in line-of-sight, it shall be more appropriate to use the less time-consuming methods.

Surface transport

Reflections on surfaces and re-evaporation are easy to implement and are usually included in models, the latter (re-evaporation) often as part of the outgassing process. Migrations on surfaces on the contrary are complex processes and there is no commercial available model.

Transport of particles

As mentioned earlier particulate transport is governed by several phenomena:

- atmospheric drag
- solar radiation pressure
- differential gravitational effects (with respect to spacecraft) which result in tide effects

- particulate charging and subsequent electrostatic effects

Among which the first three may be computed by methods similar to spacecraft orbit computing, whereas point 4 requires specific modelling to assess particulate charging in a plasma and potential map around spacecraft. The dominant phenomena are most commonly modelled: point 1, atmospheric drag, first, and also point 4 that gets important in GEO. Points 2 and 3 may become dominant in cases when points 1 and 4 become small (high altitude and no charging).

A last aspect of particulate transport is their interaction with walls. Sticking and accommodation coefficients are however very difficult to assess.

Most particulate contamination models remain in the field of research. Very few of them seem to be transferable to other users.

6.6 Specific Requirements

The external contamination requirements are based on the criticality of the mission, i.e. the sensitivity of systems (thermal blankets, solar arrays, radiators, star trackers etc.) as well as payload (optical sensors, cameras, spectrometers etc.) to contamination.

Generally the user shall:

- Perform an assessment of the system or equipment contamination sensitivity;
- Identify the contamination sources on-board;
- Evaluate, in accordance with ECSS-Q-70-01, the expected contamination levels or quantities present in critical areas, assessing the mechanisms of transport and fixation of contaminants.
- Define the modelling requirements and where quantitative levels are required use a physical outgassing and contamination transport model.

Some tentative overall external contamination requirements for the Proba3 spacecraft can be derived from previous specifications for other projects like the external contamination control requirements for the Soho. The requirements shall be such that the deposition of organic contaminants will not exceed the following level (integrated over the entire mission):

- Total molecular deposition of 30 Ångstrøm per year (this correspond to some 10^{-6}g/cm^2 or about 300ng/cm^2/year).

The requirement is intended to be achievable at minimum cost if considered early in the design, and reflect the maximum level that can be tolerated. Within the overall limit, the various spacecraft elements can be assigned contamination allocations not to be exceeded. It is important for each element not to exceed the limit in order not to cause unacceptable degradation of the overall spacecraft thermal control and power production performance. Payloads (or the proximity of such)

with e.g. cryogenic (or relatively cold sensitive surfaces) or optics (UV, visible) can pose more stringent requirements.

In order to achieve this the following guidelines shall be observed:

- Any material proposed for use and which will be exposed to space vacuum should, at a minimum, pass the outgassing requirements TML≤1% and CVCM≤0.1% when tested according to ECSS-Q-70-02 or ASTM-E595 (see section 6.5).
- Where possible, materials should be selected from ESA or NASA approved lists for space proven materials, such as ESA-PSS-1-701 (even in such cases an outgassing test may be required, depending on the criticality of the processes involved, batch to batch variability, etc.).
- In specific cases a dynamic outgassing test, such as the ESA VBQC-test or the ASTM-E1559 (see section 6.5) is required. This should, at a minimum, be done if the material used covers a surface area larger than 1000 cm^2 (this also includes any MLI materials used).

6.7 Existing Tools and Databases

Several computer codes dedicated to spacecraft contamination exist. Most of them are simulation tools at system level, but some are devoted to thruster plume modelling. Some also contain integrated (limited) data bases.

The main field of applicability of the codes is external contamination in LEO or GEO orbit. However, some programs, have limited transport modelling capabilities (simple or improved view factors only), and will give poor results in cases when return-flux through self-scatter is important.

Many the tools are also capable of analysing semi-enclosed systems. Here again, some codes can be limited due to too poor transport modelling in case of high pressures. A difference with external contamination computing for which collisional return flux may often be the main contamination process (for surfaces not in direct view), is that in closed systems direct surface to surface collisionless transport (with possible surface reflections) is most of the time the dominant process. Except for really high pressures such as 10^{-3} hPa (and thus decimetric mean free path), which may be found in semi enclosed systems yet.

For a description of available tools see [10]

Some tools include data bases about contamination effects. References to some other important data bases created independent from the tools, are found in literature:

- A data base was created by Boeing Aerospace & Electronics in 1986-1988 for Air Force Wright Research and Development Centre [11]. Its availability to non-Americans is not reported. It is a very important work resulting from the collection of over 3000 sources and covering most of contamination fields.
- The Plume Contamination Database (PCD) was developed by MMS for ESTEC, using ORACLE [12]. It is anticipated that the database is progressively filled by ESTEC

contractors and presently essentially contains measurements made at TUHH [13]. It should be available from ESA/ESTEC to the European space community.

These data bases can be used to assess contamination effects from contaminant deposit and column densities computed by the models described in the previous section.

6.8 References

[1] ECSS-Q-70-01: Contamination and Cleanliness Control

[2] ECSS-Q-70-02: A thermal vacuum test for the screening of space Materials.

[3] ASTM E-595 Method for Total Mass Loss and Collected Volatile Condensable Materials from outgassing in a vacuum environment.

[4] Van Eesbeek M. and A. Zwaal "Outgassing and contamination model based on residence time", ESA SP232, Proc. of the 3rd European Symp. on spacecraft materials in a space environment, Noordwijk, The Netherlands, 1-4 Oct 1985.

[5] ASTM E-1559 Method for contamination outgassing characteristics of space materials

[6] Dushman S., "Scientific Foundations of Vacuum Technique"; Wiley & Sons, Inc, New-York-London

[7] Scialdone J.: "Characterisation of the outgassing of spacecraft materials"; SPIE Vol. 287 Shuttle Optical Environment; 1981

[8] Trinks H.: "Exhaust Plume Databook Update Version No 3 / ESA/ESTEC Contract 7590/87/NL/TP"

[9] Simons G.A.: "Effect of Nozzle Boundary Layers on Rocket Exhaust Plumes", AIAA Journal, Tech. Notes, vol.10, No 11, 1972, pp. 1534-1535

[10] ECSS-E-ST-10-04C, Space Engineering, Space Environment

[11] Thorton & Gilbert: “Spacecraft contamination database”, SPIE Volume 13, 29; Optical System Contamination: Effects, Measurement and Control-2; 1990. pp 305-319

[12] Chéoux-Damas P., Théroude C., Castejon S., Hufenbach B., PCD: An interactive tool for archiving plume impingement and contamination data, The Proceedings of the Second European Spacecraft Propulsion Conference, ESTEC, Noordwijk, The Netherlands, May 27-29, 1997, p. 587-594

[13] Trinks H., Surface Effect Data Handbook (SEDH III), Report V, ESA Contract No 7510/87/NL/PP, Sept. 1991